



HAL
open science

Accretion and subduction mass transfer processes: Zircon SHRIMP and geochemical insights from the Carboniferous Western Series, Central Chile

Jesus Munoz-Montecinos, Aitor Cambeses, Samuel Angiboust

► To cite this version:

Jesus Munoz-Montecinos, Aitor Cambeses, Samuel Angiboust. Accretion and subduction mass transfer processes: Zircon SHRIMP and geochemical insights from the Carboniferous Western Series, Central Chile. *International Geology Review*, 2023, Subduction, accretion, and collision in Latin America, the Caribbean, and Iberia: a tribute to the career of Antonio García-Casco, 66 (1), pp.54-80. 10.1080/00206814.2023.2185822 . hal-04815953

HAL Id: hal-04815953

<https://hal.science/hal-04815953v1>

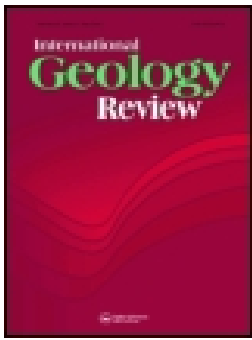
Submitted on 3 Dec 2024

HAL is a multi-disciplinary open access archive for the deposit and dissemination of scientific research documents, whether they are published or not. The documents may come from teaching and research institutions in France or abroad, or from public or private research centers.

L'archive ouverte pluridisciplinaire **HAL**, est destinée au dépôt et à la diffusion de documents scientifiques de niveau recherche, publiés ou non, émanant des établissements d'enseignement et de recherche français ou étrangers, des laboratoires publics ou privés.



Distributed under a Creative Commons Attribution - NonCommercial - NoDerivatives 4.0
International License



Accretion and subduction mass transfer processes: Zircon SHRIMP and geochemical insights from the Carboniferous Western Series, Central Chile

Jesus Munoz-Montecinos, Aitor Cambeses & Samuel Angiboust

To cite this article: Jesus Munoz-Montecinos, Aitor Cambeses & Samuel Angiboust (2023): Accretion and subduction mass transfer processes: Zircon SHRIMP and geochemical insights from the Carboniferous Western Series, Central Chile, International Geology Review, DOI: [10.1080/00206814.2023.2185822](https://doi.org/10.1080/00206814.2023.2185822)

To link to this article: <https://doi.org/10.1080/00206814.2023.2185822>



© 2023 The Author(s). Published by Informa UK Limited, trading as Taylor & Francis Group.



[View supplementary material](#)



Published online: 07 Mar 2023.



[Submit your article to this journal](#)



[View related articles](#)



[View Crossmark data](#)

Accretion and subduction mass transfer processes: Zircon SHRIMP and geochemical insights from the Carboniferous Western Series, Central Chile

Jesus Munoz-Montecinos ^{a,b,c}, Aitor Cambeses ^{a,b,d} and Samuel Angiboust^{a,e}

^aInstitut de Physique du Globe de Paris, Université de Paris, Paris, France; ^bDepartment of Mineralogy and Petrology, Faculty of Sciences, University of Granada, Granada, Spain; ^cDepartment of Earth Sciences, Structural Geology and Tectonics Group, Geological Institute, Zürich, Switzerland; ^dInstitut für Geologie, Mineralogie & Geophysik Ruhr-Universität, Bochum, Germany; ^eEcole Normale Supérieure of Lyon, Lyon University, Lyon, France

ABSTRACT

In the region of Pichilemu (Central Chile), the exhumed roots of the Carboniferous paleo-accretionary wedge developed during subduction of an oceanic realm underneath the western Gondwana margin are exposed. We focus on the areas of Infiernillo beach and Punta de Lobos: the former representing a well-characterized transitional blueschist-facies coherent stack of metabasitic lithologies interlayered at the centimetre- to metre-scale within metasedimentary rocks and glaucophanites, whereas the latter corresponds to a massive, up to hundreds of metres thick, strained metapillow lavas edifice surrounded (not interlayered) by metasedimentary rocks. We provide new field, geochemical, Raman thermometry and zircon SHRIMP U-Th-Pb geochronology on the lithologies forming the Infiernillo-Punta de Lobos complex aiming at characterizing the sedimentary sources and the extent of mechanical mixing. Field observations suggest that the Infiernillo-Punta de Lobos complex can be considered as part of the same successions, subducted and basally accreted almost coherently at high pressure-low temperature (HP-LT) conditions. The geochemistry signal in metasedimentary rocks and maximum deposition ages point to a marked forearc source for all the metasedimentary and glaucophanite lithologies, whereas massive metapillow lavas and greenschists might represent volcanic products and oceanic roughnesses erupted near the trench when the oceanic material approached the Gondwana margin at c. 329 Ma. It is suggested that the interlayering now observed in the field is mostly the consequence of sedimentary and/or volcanic processes close to the trench environment, with minor tectonic reworking of the pre-subduction structures (e.g. lithological contacts). Our results suggest that the Punta de Lobos edifice is closely related to the subduction of large volumes of continent-derived, trench-filling sediments towards HP-LT conditions. Thus, in line with previous experimental and numerical simulations, we emphasize the potential role of oceanic roughness as stress perturbations that could contribute to the subduction of thick sedimentary sequences, and discuss their implications for seismogenesis.

ARTICLE HISTORY

Received 17 February 2022
Accepted 25 February 2023



KEYWORDS

Western Series; zircon geochronology; basal accretion; subduction; sedimentary recycling; seamounts


1. Introduction

Mass transfer processes in subduction zones depend to a large extent on their tectonic behaviour, characterized by accretionary- or erosion-dominated regimes (Cloos and Shreve 1988; Stern 2002; Scholl and von Huene 2010). In the former case, the sediments capping the oceanic crust are frontally accreted and underplated at shallow levels (typically <10 km depth; e.g. Glodny *et al.* 2005; von Huene *et al.* 2021) and/or basally accreted at greater depths (typically in the range of 20–45 km depth; Grove and Bebout 1995; Calvert *et al.* 2006; Hyppolito *et al.* 2016; Xia and Platt 2017; see also Angiboust *et al.* 2022 for a review). Conversely, the erosive margins are characterized by the consumption of the forearc crust

until the complete destruction of the former accretionary wedge, even affecting ancient batholites in the most abrasive cases (Clift and Vannucchi 2004; Kukowski and Oncken 2006; Kay *et al.* 2014; Angiboust *et al.* 2017, 2018). The occurrence of one or the other regime is thought to be controlled by the topography of the subducting oceanic plate (e.g. seamounts, ridges; Miura *et al.* 2004; Ruh *et al.* 2016; Angiboust *et al.* 2022), relative rates of plate convergence (Clift and Hartley 2007; Behr and Becker 2018) and sediment availability (Moore and Saffer 2001). Although the mutual feedbacks between these various parameters remain to be clarified, it is accepted that subducting sediments are frictionally weak (Tobin and Saffer 2009). Thus, variations in

CONTACT Jesus Munoz-Montecinos  jmunoz@erdw.ethz.ch  Department of Earth Sciences, Structural Geology and Tectonics Group, Geological Institute, Zürich, Switzerland

This article has been corrected with minor changes. These changes do not impact the academic content of the article.

 Supplemental data for this article can be accessed online at <https://doi.org/10.1080/00206814.2023.2185822>

© 2023 The Author(s). Published by Informa UK Limited, trading as Taylor & Francis Group.

This is an Open Access article distributed under the terms of the Creative Commons Attribution-NonCommercial-NoDerivatives License (<http://creativecommons.org/licenses/by-nc-nd/4.0/>), which permits non-commercial re-use, distribution, and reproduction in any medium, provided the original work is properly cited, and is not altered, transformed, or built upon in any way.

sediment supply, e.g. due to climatic factors (Lamb and Davis 2003; Hu *et al.* 2021), along with the occurrence of oceanic roughness translate into changes in the mechanical coupling of the subduction interface. These variations eventually affect the shear stresses and allow a switch between erosion- and accretionary-dominated regimes (Angiboust *et al.* 2022 and references therein).

In the geological record, basal accretion processes have been documented in many paleo-subduction complexes worldwide, ultimately resulting in the exhumation of high-pressure (HP) metamorphic rocks (Glodny *et al.* 2005; Richter *et al.* 2007; Raimbourg *et al.* 2014; Wakabayashi 2017; Angiboust *et al.* 2018; Tewksbury-Christle and Behr 2021) undefined. However, a small fraction of the subducted material decouples from the subducting slab and is underplated to the hanging wall (e.g. Platt 1993; Ring and Layer 2003; Clift and Vannucchi 2004). Such dynamics commonly obliterate the original accretionary sequence, especially at higher metamorphic degrees, making it challenging to document the physical nature of the subduction interface (Angiboust *et al.* 2022 and references therein). From a geophysical perspective, underplating and basal accretion have been imaged in several subduction zones (e.g. Ye *et al.* 1997; Calvert *et al.* 2006; Hicks *et al.* 2012; Moreno 2018; Ramos *et al.* 2018; Wakita 2019), demonstrating that sediments are the major constituent involved in such process, as also documented in exhumed paleo-subduction complexes (e.g. Willner *et al.* 2004; Glodny *et al.* 2005; Ernst 2011; Creixell 2016; Tewksbury-Christle and Behr 2021).

The mechanics controlling accretionary processes at the frontal and basal accretion sites in subduction settings have been for several decades a matter of numerous investigations (Lallemand *et al.* 1992; Kukowski *et al.* 1994; Glodny *et al.* 2005; Ruh *et al.* 2012; Noda *et al.* 2020). In accretionary regimes such as in Chilean-type margins (Stern 2002), the progressive growth of the frontal accretionary prism by sediment accretion results in the thinning of the subduction channel inhibiting subduction of continent-derived material towards HP-LT conditions (Cloos and Shreve 1996). To explain the occurrence of continent-derived material subducted to blueschist-facies conditions or beyond, Noda *et al.* (2020) demonstrated, by means of analogue modelling, that the subduction of stiff oceanic reliefs promote transient widening of the subduction channel and further detachment of sediments on their surroundings, thus enhancing underplating (see also Lallemand *et al.* 1994; Ruh *et al.* 2016). These results are supported by seismic reflection studies in active subduction settings where subducted sediments have been imaged in close

association with oceanic reliefs (e.g. Li 2018). In contrast, the lack of topographic reliefs during subduction results in the growth of the frontal accretionary wedge narrowing the subduction channel and making it less optimal for continent-derived sediment mass transfer to HP conditions.

All these processes occur in a depth range where megathrust earthquakes and episodic tremors and slips are reported in modern subduction settings (e.g. Obara *et al.* 2004; Moreno *et al.* 2014; Behr and Bürgmann, 2020). Furthermore, the occurrence of sedimentary, commonly fluid-saturated materials capping the mafic oceanic crust, critically affects the rheological properties of the subduction interface, ultimately controlling the topographic expression of the forearc (Bassett and Watts 2015; Menant *et al.* 2019, 2020; Sun *et al.* 2020; Delph *et al.* 2021). While numerical modelling studies clearly demonstrate a major impact of topographic asperities on plate interface dynamics, new field evidence documenting the potential tectonic impact of deep seamount subduction onto accretionary dynamics is lacking.

In order to decipher the nature and architecture of the interface-forming lithologies at depths compatible with a variety of seismic and aseismic processes, it is crucial to gain *in situ* insights onto the material forming the subduction channel. We herein focus on the transitional blueschist-facies sequences of Infiernillo and Punta de Lobos (Western Series, Pichilemu region, Central Chile). We provide new geochronological and thermometric constrains together with geochemical analyses to characterize the nature of the meta-volcano-sedimentary materials forming the metamorphic pile, which has to a great extent escaped exhumation-related overprinting (Muñoz-Montecinos *et al.* 2020). Zircon age distribution patterns along with geochemical analyses provide the opportunity to illuminate the source of the material and their likely distribution in the original volcanosedimentary pile. This approach sheds a new light onto tectonic mixing and crustal recycling processes and their relationships with the mechanical properties of the subducted slab, confirming the importance of the Pichilemu region as a key natural laboratory for understanding plate interface dynamics.

2. Geological setting

The late Palaeozoic subduction of oceanic crust beneath the western continental margin of Gondwana resulted in the formation of the high pressure-low temperature (HP-LT) 'Western Series' (Hervé 1988). This metamorphic belt is believed to represent the ancient remnants of the

lapetus Ocean that once separated Gondwana from Laurentia (Dalziel 1991; Dahlquist *et al.* 2021). It is speculated that the continental basement of the southwestern margin of Gondwana, in the latitudes of present-day central Chile (e.g. 30° to 38° S), resulted from the accretion of the exotic terranes Cuyania and Chilenia, which are believed to have collided during Ordovician and Devonian times, respectively (Ramos *et al.* 1986; Thomas and Astini 2003; Ramos 2004; Massonne and Calderón 2008; Willner *et al.* 2011; Heredia 2018 references therein; Hervé *et al.* 2020). Conversely, Dahlquist *et al.* (2021 and references therein) suggest that the configuration of this region during the late Palaeozoic was dominated by changes in subduction geometry (e.g. from slab roll-back to flat-slab) rather than collisional tectonics.

The present-day Western Series represent an almost continuous, N-S oriented belt that constitutes part of the Chilean Coastal Cordillera and is composed of continent-derived metasedimentary rocks interspersed within rare oceanic metavolcanics (Hervé 1988; Willner 2005; Hyppolito *et al.* 2014). Maximum pressure-temperature (P-T) estimates along different locations belonging to the Western Series yielded amphibolite- to incipient eclogite-facies burial conditions; resulting in burial depths up to c. 60 km in the subduction channel (e.g. Los Pabilos: Kato *et al.* 2008; Punta Sirena: Hyppolito *et al.* 2014 La Cabaña: Plissart 2019). In the region of Pichilemu (34° 23' 30" S, 72° 01' 30" W), specifically at the beach of Infiernillo and Punta de Lobos locality (Figures 1a-c), rocks representing former remnants of the Carboniferous subduction on the southwestern active margin of Gondwana, outcrop now in the Western Series. The sequence corresponds to a coherent stack of pelagic and continent-derived metasedimentary, metaproclastic rocks and to lesser extent, metalavas and metapillow lavas (Hervé 1988; Willner *et al.* 2005; Hyppolito *et al.* 2014). The metavolcanic materials documented in Pichilemu have been classified as E-MORB, N-MORB and OIB (e.g. Hervé *et al.* 1984; Willner 2005). The latter signature is characteristic of Infiernillo metavolcanics and interpreted as scraped off slices of the uppermost section of the subducted slab (Willner 2005; Hyppolito *et al.* 2014). The main tectonic structure is a NE-NNE striking, penetrative transposition main foliation S2 dipping from sub-horizontal to sub-vertical that overprinted previous subduction-related structures (e.g. S1 foliation). ⁴⁰Ar/³⁹Ar plateau ages in phengite crystals lining the main foliation in blueschists and metapsammopelites from the Western Series range between 292 ± 1 Myr and 320 ± 1 Ma, and are interpreted as dating the HP basal accretion stage and the development of the transposition main foliation (Willner *et al.* 2005). The

same method applied in phengite in microfolds resulted in ages ranging from 260 to 308 Ma, interpreted as dating the retrograde crystallization during cooling and exhumation (Willner *et al.* 2005). The metabasites yielded peak metamorphic conditions of 0.75–0.80 GPa at 380–420°C (Hyppolito 2014; Figure 1d) followed by an incipient greenschist-facies overprint (Hyppolito 2014). The HP-LT events were contemporaneous with the intrusion of arc-related granitoids at c. 330 to 300 Ma (U-Pb zircon; Willner *et al.* 2005; Deckart *et al.* 2014; Creixell *et al.* 2021), which are thought to have provided heat for the low pressure-high temperature (LP-HT) metamorphism recorded in the Eastern Series. The latter represents former passive margin sediments frontally accreted to the accretionary wedge at c. 340 Ma (Aguirre *et al.* 1972; Hervé 1988; Glodny *et al.* 2008; Hervé *et al.* 2013; Hyppolito *et al.* 2014). The end of the magmatic activity is recorded by lately intruding granitoids that yielded U-Pb and Rb-Sr ages from 257 to 220 Ma (mineral and whole rock; Lucassen *et al.* 2004; Willner *et al.* 2005) and have been associated with the retreat of the subducting slab.

3. Characterization of the Infiernillo and Punta de Lobos complex

The metavolcanosedimentary sequence of Infiernillo has been previously subdivided into three cofacial coherent units (Hyppolito 2014; Muñoz-Montecinos *et al.* 2020; Figures 1d, 2a and 3a). The blue-green schists correspond to a metavolcanic sequence including metalavas, metapillow lavas, metatuffs, metalapilli-tuffs and glaucophanites (Figures 3(b,c)). Their characteristic NE-NNE S2 fabrics is more penetrative in the metaproclastic rocks and less developed in metalavas. Blueschists are fine-grained rocks scarcely affected by retrogression. Their penetrative S2 foliation is characterized by oriented grains of glaucophane (locally riebeckite), winchite and actinolite along with albite, chlorite, phengite, rutile, titanite and apatite as well as rare epidote and quartz. Amphibole displays zoning patterns characterized by hornblende cores, actinolitic mantles and glaucophane rims. Glaucophane rimming actinolite is interpreted as a prograde crystallization sequence (Muñoz-Montecinos *et al.* 2020). Greenschist lithologies contain the same mineral phases but with higher abundance of chlorite over amphibole and albite, but the dominant amphibole species is indeed actinolite rather than glaucophane. Intermediate compositions containing winchite as the dominant amphibole species are also common. Thus, based on field observations and thermodynamic modelling, Muñoz-Montecinos *et al.* (2020) inferred that either blueschists and greenschists, as well as intermediate lithologies are co-facial and that

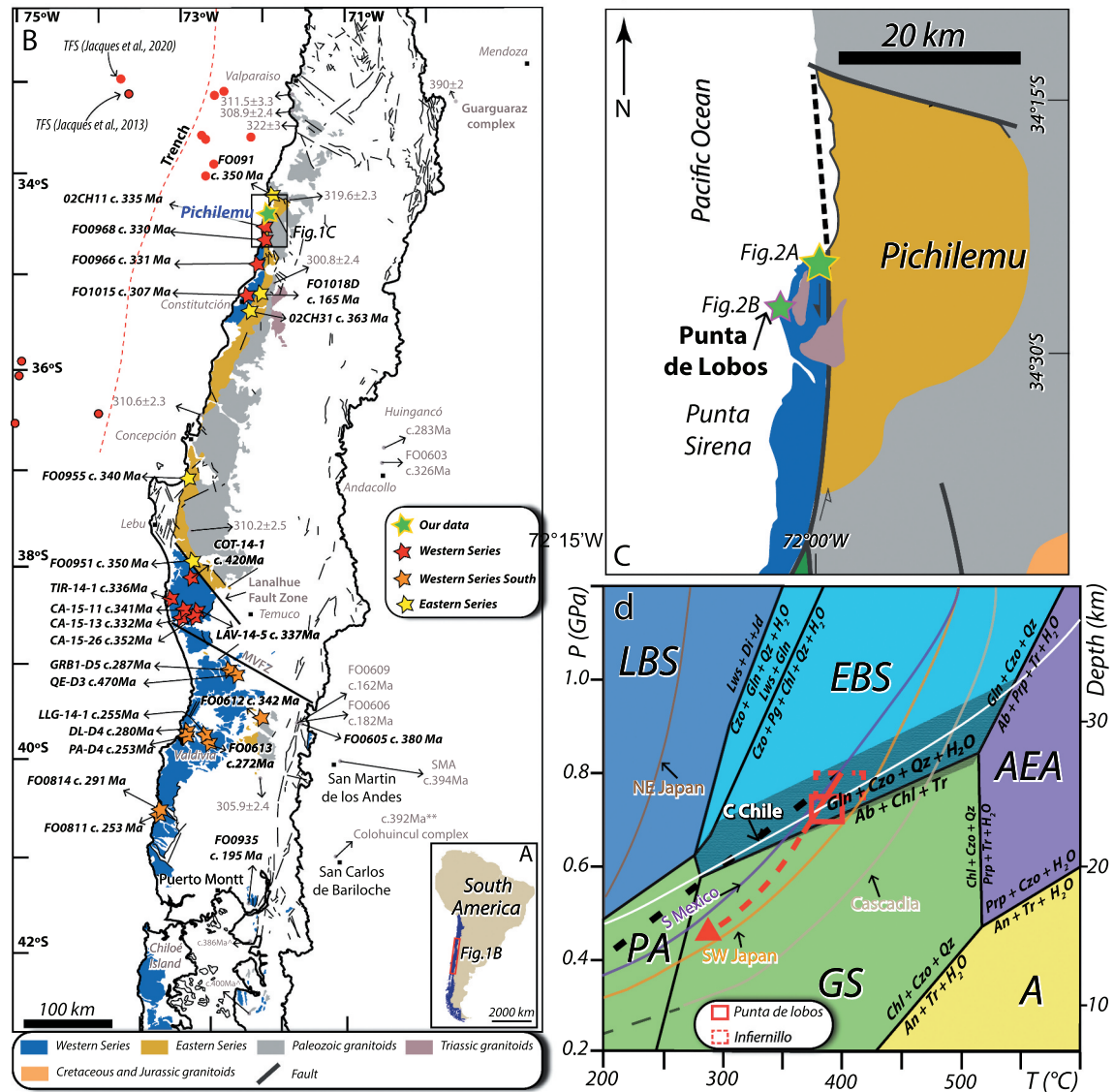


Figure 1. (a) Location of the studied region relative to South America. (b) Geological map of the studied zone and further south showing reported maximum deposition (black bold) and crystallization ages (light grey), respectively (modified from Hervé *et al.* 2013, 2020; see references therein). (c) Simplified geological map of the Pichilemu region, central Chile. (d) Pressure-temperature (P-T) diagram (modified from Muñoz-Montecinos *et al.*, 2020) representing inferred peak and retrograde metamorphic conditions for the blue-green schists at Infernillo (red dashed box and arrow after Hyppolito 2014). The dashed black line corresponds to a subduction thermal gradient of 15°C/km. For comparison, the subduction thermal gradients from Cascadia, Japan and Mexico (after Peacock *et al.* 2002) and central Chile (after Ji *et al.* 2019) are shown. The background fields and the grey-shaded region, the latter corresponding to overlap among stability fields, are from Evans (1990). PA – pumpellyite-actinolite facies; GS – greenschist facies; A—amphibolite facies; AEA – albite-epidote amphibolite facies; EBS – epidote-blueschist facies; LBS – lawsonite blueschist facies; TFS – trench-filling sediments. Mineral abbreviations from Whitney and Evans (2010).

the occurrence of one or the other mineral assemblage is due to major elements' variations, mostly in $Mg/(Me+Fe^{2+})$ ratios as well as Al, Ca and Na. It was concluded that the occurrence of centimetre to metre-scale layering of blueschists and greenschists could be interpreted as local bulk rock compositional variations that likely occurred as primary heterogeneities in the igneous protoliths and sea-floor hydrothermal alteration (Muñoz-Montecinos *et al.* 2020). The glaucophanites correspond to blueish, very

fine-grained rocks intercalated at the centimetre-scale within metavolcanic materials. They display extremely sharp contacts with other lithologies and are oriented parallel to sub-parallel to the main fabric of the complex. There is no evidence of reaction halo or mineralogical gradients in the rocks adjacent to the glaucophanites.

The dark phyllites unit is a fine to very fine-grained metasiliclastic pelagic-hemipelagic sequence including dark phyllites with abundant organic matter. Rare lenses

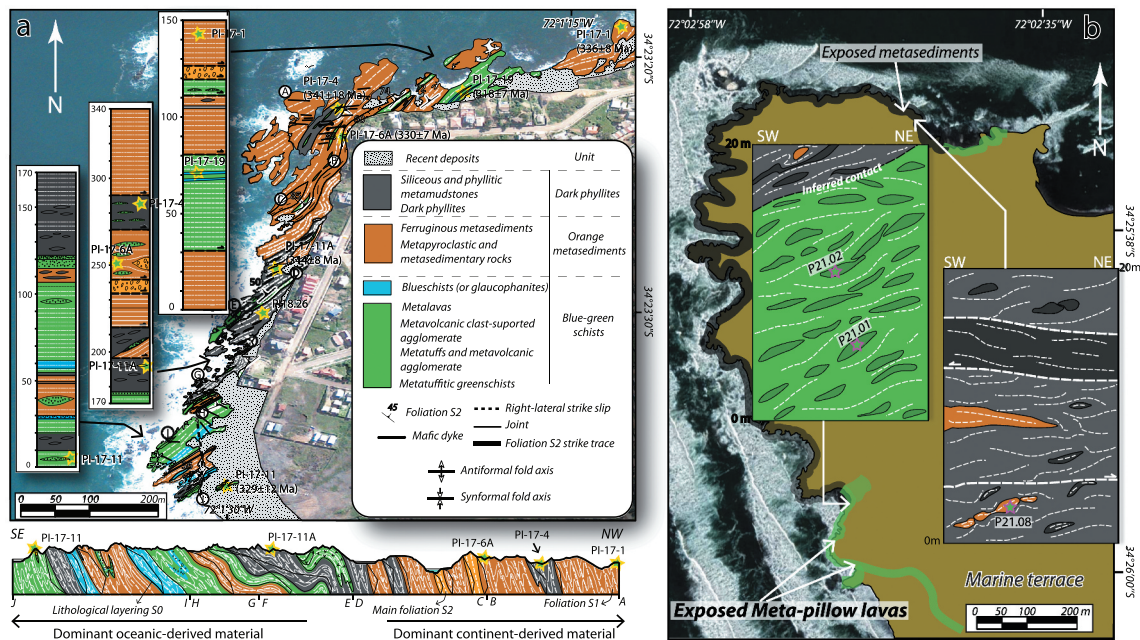


Figure 2. Geological maps and cross-section profiles of the Infiernillo (a) and Punta de Lobos (b) localities. Latitude and longitude coordinates are shown. The stars correspond to the samples obtained for this study. The ages displayed in the panel a correspond to the maximum sedimentation ages. The panel a has been modified from Hyppolito *et al.* (2014).

of blue-green schists are embedded within the phyllitic matrix. The largest unit in terms of area corresponds to the orange metasedimentary rocks, which is composed mainly of metasandstones, metaconglomerates, quartzites, metacherts, ferruginous metasedimentary and felsic metapyroclastic rocks (Figure 3d). There is a strong grain size heterogeneity, ranging from fine-grained in quartzites to coarse-grained in metaconglomerates, the latter including andesitic to dacitic volcanic fragments. In the Western Series, Willner (2005) inferred that rocks of this type represent former trench-filling sediments supplied from the continental crust. Overall, both metasedimentary lithological units, and to a lesser extent the blue-green schists, exhibit a well-developed S2 foliation. In the metasedimentary rocks, fringes of insoluble material occur along the main foliation, indicating that dissolution-precipitation mechanism was active during deformation (Muñoz-Montecinos *et al.* 2020). The S1 foliation is preserved within the S2 fabric defining intrafolial folds whose axial planes, and in consequence the S2 planes, are oriented slightly oblique to the main lithological layering (S0 fabric; see the cross-section panel from Figure 1a). The former S2 main foliation is overprinted by the S3 fabric, which is oriented at high angles (nearly perpendicular) with respect to the S2.

At Punta de Lobos locality (c. 5 km south of Infiernillo; Figure 1c), abundant phyllites outcrop. This sequence is comparable to the dark phyllites sequences from Infiernillo beach (Figures 2b and 3e). At Punta de

Lobos, a several metres-thick diabase sill occurs devoid of subduction-related metamorphic overprint (see below). Minor metasandstones and quartzites lenses comparable to the orange metasediments from Infiernillo are interbedded within the dark phyllites (Figures 2b and 3e). Towards the southwestern part of Punta de Lobos, a massive and coherent sequence of strongly strained metalavas and metapillow lavas outcrops (Figures 3f-h). Although the tectonic contact between the dark phyllites and the metavolcanic massif has not been observed, we infer that the latter is overlain by the dark phyllites (Figure 2b). Hyppolito *et al.* (2014) classified this metapillow lava sequence as a plume-influenced OIB-EMORB volcanic body, potentially representing an oceanic topographic high near the western margin of the Chilenia microplate. Thermobarometric studies on a greenschist sample from this metapillow lava body yielded peak burial metamorphic conditions of 0.70–0.75 GPa at 370–400°C (Figure 1d), followed by a cryptic higher temperature event at slightly shallower depths (c. 0.65 GPa at 570°C), possibly associated with the emplacement of Triassic intrusive bodies (e.g. the diabase sill; Hyppolito 2014). This thermal anomaly has not been detected in the Infiernillo sequence.

All the sequences exposed at Punta de Lobos gently dip towards the NW-SE with variable strike orientations, ranging from NNE to NNW due to high wavelength folding of the entire metamorphic stack. The internal structure of the massif is not well visible since it is

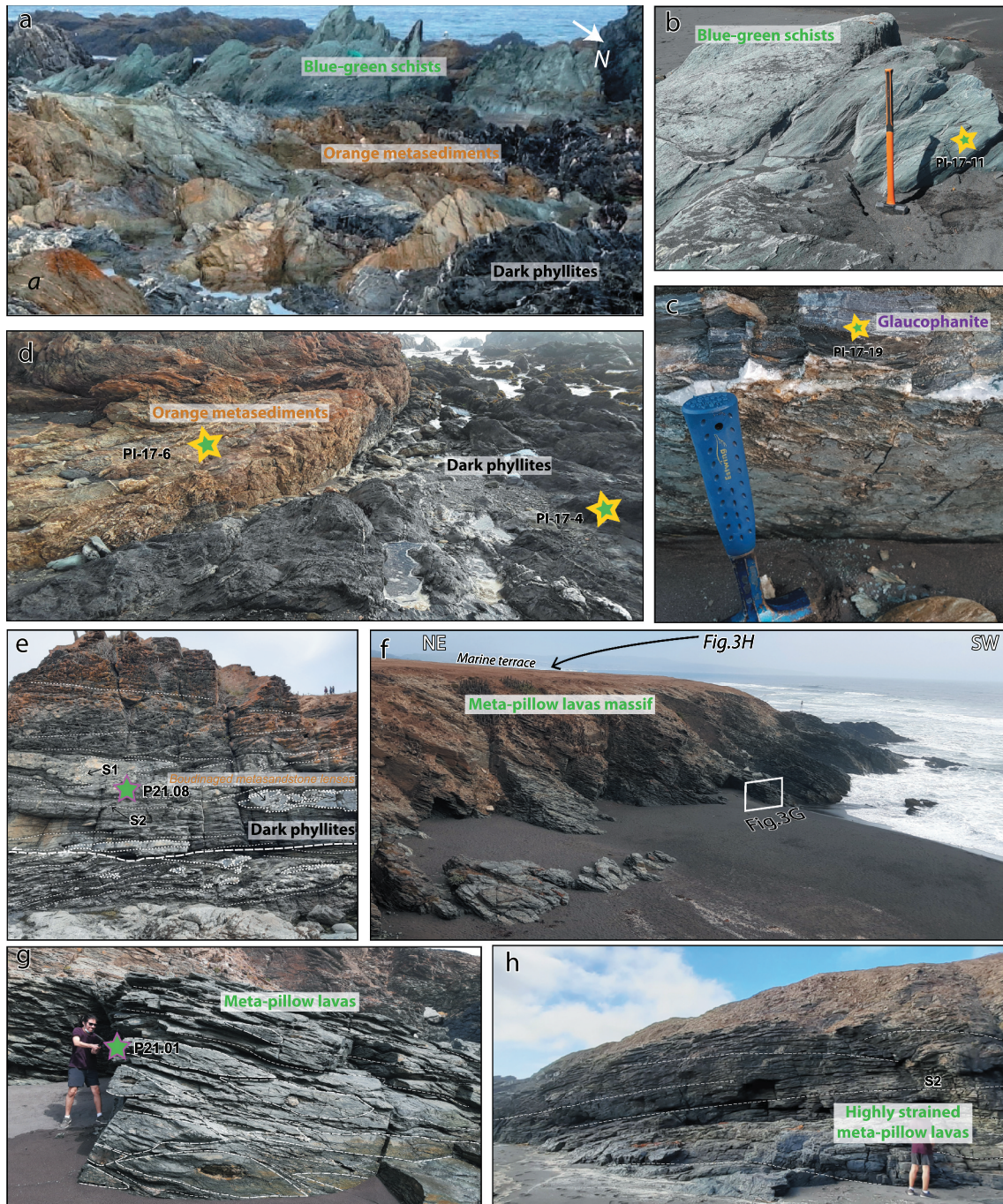


Figure 3. Representative field views of Infernillo (a to d) and Punta de Lobos outcrops (e to h). (a) General structural relationships between the blue-green schists, dark phyllites and orange metasediments. (b) View of a representative blue-green schists outcrop. (c) Detailed view of a glaucophanite interlayered in the blue-green schists. (d) Contact between the orange metasediments and dark phyllites; note the sharp lithological contact among the units. (e) General view of the dark phyllites and associated orange metasediment lenses. (f) General view of the Punta de Lobos metapillow lavas massif. (g) Close-up of the Punta de Lobos metapillow lavas. (h) Highly strained metapillow lavas; the maximum flattening orientation is parallel to the main foliation S2. The stars represent spots where the samples have been extracted.

covered by fluvial-marine sedimentary deposits (Pleistocene-Holocene?) and marine erosional terraces, which are also affected by regional-scale normal faulting (e.g. Pichilemu Fault; see Aron *et al.* 2012). Intrafolial folds (F2) observed in the metavolcanic and

metasedimentary lithologies (Figure 3e) indicate the presence of a pre-peak subduction-related deformation event (S1) overprinted by a later pervasive transposition main foliation S2, locally overprinted by the S3 fabric (crenulation cleavage). The pillow structures in the

greenschist metavolcanics are strongly strained with the maximum stretching direction parallel to the dip direction of the main foliation S2 (Figures 3g-h). In addition, boudinaged orange metasediment bodies wrapped by the dark phyllites highlight viscosity contrasts among the different units (see Muñoz-Montecinos *et al.* 2020 for similar observations at the Infiernillo beach). The strikingly similar lithological, deformational, and peak P-T conditions (see Hyppolito 2014) reached by Punta de Lobos lithologies allow us to correlate this sequence with the Infiernillo complex, both possibly representing a single metamorphic stack (hereafter referred to as the Infiernillo-Punta de Lobos complex).

In the Infiernillo-Punta de Lobos complex, shear bands are commonly observed within individual units, particularly within the dark phyllites (e.g. Figure 3e). However, we note that the contacts between the different units are, in general, sharp and clean, with no significant evidence of increased shearing intensity, cataclastic shear bands or grain size reduction towards the different lithological units. We emphasize that no cataclasites, ultracataclasites or pseudotachylites were observed in the field, despite a thorough examination. The entire Infiernillo-Punta de Lobos complex was affected by the same deformation history, namely (i) the strong flattening of the units, including rigid objects such as pillows and veins, and (ii) the formation of the transposition main foliation that likely occurred after basal accretion at c. 25 km depth in the transitional blueschist-facies field (e.g. Glodny *et al.* 2005; Richter *et al.* 2007; Hyppolito 2014; Muñoz-Montecinos *et al.* 2020; Figure 1D). The high-pressure stage was followed by deep duplex exhumation (e.g. Willner 2005) in the fore-arc region allowing the formation of post-subduction-related structures (e.g. F3 and S3).

4. Analytical methods

4.1 Whole rock geochemistry

Five glaucophanites (Infiernillo), along with two metapillow lavas and one orange metasediment samples (Punta de Lobos) were crushed and pulverized for major and trace element determinations using X-Ray fluorescence (XRF) and inductively coupled plasma mass spectroscopy (ICP-MS) at the Centro de Instrumentación Científica from the Universidad de Granada (CIC-UGR). For XRF determinations, the samples were melted within a lithium tetraborate fusion flux resulting in a typical precision better than $\pm 1.5\%$ for an analyte concentration of 10 wt%. Zirconium concentrations were determined using the same methodology. ICP-MS trace element determinations were carried out after $\text{HNO}_3 + \text{HF}$

digestion of 0.1 g of pulverized sample in a Teflon-lined vessel at 180°C for 30 min. It was followed by evaporation to dryness and further dissolution in 100 mL of HNO_3 (4 vol%). Precision for this methodology is generally better than $\pm 2\%$ for an analyte concentration of >50 ppm and $\pm 5\%$ for an analyte concentration of >5 ppm. The results are shown in Supp. Table S1.

4.2 Zircon SHRIMP analysis

Zircon crystals were separated from representative lithologies belonging to each of the exposed units at Infiernillo (see sample location in Figure 2a): two samples from the blue-green schists, a greenschist (PI-17-11) and a glaucophanite (PI-17-19); and two samples from the dark phyllites (PI-17-4, PI-17-11A) and two samples from the orange metasediments (PI-17-1, PI-17-6A). We tentatively separated zircons from 20 kg of Punta de Lobos metapillows but the number of crystals was too low to undertake an appropriate geochronological study on this material. Zircon crystals were separated using panning; first in water and then in ethanol, followed by magnetic extraction of Fe-rich minerals with a Nd magnet. Finally, zircon crystals were handpicked using a binocular microscope. The zircon grains were cast on 'megamounts', i.e. 35 mm epoxy discs fixed on the front of a mount holder, so that no metallic parts or surface discontinuities faced the secondary ions extraction plate. The minerals were carefully studied with optical (reflected and transmitted light) and scanning electronic microscopy (backscattering and cathodoluminescence) prior to SHRIMP analyses.

Zircon crystals were analysed at the CIC-UGR with the IBERSIMS SHRIMP IIe/mc ion microprobe for U-Th-Pb following the method described by Williams & Claesson (1987). The mount was coated with a ≈ 12 nm thick gold layer. Each spot was rasterized with the primary beam for 120 seconds prior to analysis, and then analysed for 6 scans following the isotope peak sequence $^{196}\text{Zr}_2\text{O}$, ^{204}Pb , $^{204.1}$ background, ^{206}Pb , ^{207}Pb , ^{208}Pb , ^{238}U , ^{248}ThO , ^{254}UO . Each peak of each scan was measured sequentially 10 times, with the following total counting times per scan: 2 s for mass 196; 5 s for masses 238, 248, and 254; 15 s for masses 204, 206, and 208; and 20 s for mass 207. The primary beam, composed of $^{16}\text{O}^{-16}\text{O}^+$, was set to an intensity of about 5 nA, with two Köhler apertures: (1) at 120 μm and (2) at 70 μm , which generated 17×20 and 9×12 μm elliptical spots on the target to analyse cores and rims, respectively (see section 6). The secondary beam exit slit was fixed at 80 microns, achieving a resolution of about 5000 at 1% peak height. All calibration procedures were performed on the standards included on the same mount. Mass calibration was

done on the REG zircon (ca. 2.5 Ga, very high U, Th and common lead content). The analytical session started by measuring the SL13 zircon (Claoué-Long *et al.* 1995), which was used as a concentration standard (238 ppm U). The TEMORA zircon (416.8 ± 1.1 Ma; Black *et al.* 2003), used as an isotope ratios standard, was then measured every 4 unknowns. Data reduction was done with the SHRIMPTOOLS software (available at www.ugr.es/~fba), which is a new implementation of the PRAWN software originally developed for the SHRIMP. Errors are reported at the 95% confidence interval ($\approx 2 \sigma$). Standard errors (95% C.I.) on the 37 replicates of the TEMORA standard measured during the analytical session were $\pm 0.35\%$ for $^{206}\text{Pb}/^{238}\text{U}$ and $\pm 0.83\%$ for $^{207}\text{Pb}/^{206}\text{Pb}$.

4.3 Raman thermometry on metasedimentary rocks

Two samples from the dark phyllites unit belonging to distinct lenses from the Infernillo-Punta de Lobos complex were selected to conduct Raman spectroscopy of carbonaceous materials (RSCM) thermometric studies based on the gradual graphitization of organic matter (Beysac *et al.* 2002). This geothermometer enables the characterization of the maximum temperature reached by a geological sample (in the range 330–600°C) with an absolute accuracy of $\pm 50^\circ\text{C}$. Spectra were measured at the Geology laboratory of Ecole Normale Supérieure (Paris) using a Renishaw InVia Raman spectrometer following the procedure described by Beysac *et al.* (2002). Thirteen and twenty spectra were acquired on samples P18.26 and PI-17-11A, respectively. The resulting spectra were treated with the software Peakfit.

5. Petro-geochemical constraints on accreted materials

In this section, we focus on characterizing the glaucophanites as well as the metavolcanosedimentary material encountered in the field since no detailed studies have been carried out on these lithologies so far. The oceanic-derived blueschist-greenschist metabasites (blue-green schists) have been previously described in detail by Hyppolito *et al.* (2014), Halama and Konrad-Schmolke (2015) and Muñoz-Montecinos *et al.* (2020).

The glaucophanites, which are only found in the Infernillo beach, consist of a homogeneous fine to very fine-grained aggregate of glaucophane (up to 90 vol%) + albite and minor, rutile, titanite, phengite and zircon. Rare hornblenditic cores have been observed in amphibole crystals rimmed by glaucophane. Albite porphyroblasts are partially to totally replaced by

glaucophane, the latter defining the penetrative S2 fabric. The main difference between this lithology and the blueschists is that the former contains virtually only glaucophane while the latter is a mixture of glaucophane along with winchite, chlorite, albite and epidote. The orange metasediments from Infernillo-Punta de Lobos are heterogeneous, including well- to poorly-sorted quartzites, metasandstones, polymictic metaconglomerates, and locally metabreccias. Their mineralogy is, in general, characterized by phengite, which defines the main foliation as well as abundant quartz, stilpnomelane, iron oxides and albite. Chlorite is locally present along with minor zircon. At the Infernillo locality, the great abundance of stilpnomelane gives these rocks their characteristic orange tints. The dark phyllites are strongly foliated homogeneous rocks containing fine-grained white mica, chlorite, quartz, organic matter and minor albite, pyrite, titanite and zircon. In these lithologies, a moderate crenulation cleavage is often visible while dark seams and organic matter fringes are present along foliation planes. RSCM calculations on the organic material from the dark phyllites yield average temperatures of $412 (\pm 14^\circ\text{C } 1-\sigma)$ and $396 (\pm 19^\circ\text{C } 1-\sigma)$ for the samples P18.26 and PI-17-11A, respectively.

In terms of major elements, SiO_2 in the glaucophanitic lithologies (see Table S1) ranges from 61 to 68 wt%; Al_2O_3 from 9 to 15 wt%; and $\text{Mg}/(\text{Mg}+\text{Fe}^{2+})$ from c. 0.4 to 0.5. Thus, these samples are mostly trachytic and, to a lesser extent, dacitic in composition (without a petrogenetic sense). The orange metasediments are the richest in SiO_2 with values ranging from 72 to 91 wt%, as would be expected in a quartz-rich lithology, while the dark phyllites range from 59 to 69 wt% (see Table S1 and Muñoz-Montecinos *et al.* 2020). According to $\text{SiO}_2/\text{Al}_2\text{O}_3$ vs $\text{Fe}_2\text{O}_3/\text{K}_2\text{O}$ (Figure 4a) ratios, all dark phyllite samples and one glaucophanite can be considered as greywackes, while the orange metasediments plot in the field of litharenite and sublitharenites. The rest of the glaucophanites correlate well with sandstone-related compositions. Most worldwide trench-filling sediments (Plank 2014) plot in the greywacke and shale fields with minor litharenite, sandstone and sublitharenite signatures. It is worth noticing that arc-derived trench-filling sediments sampled south of Pichilemu (Jacques 2013; Figures 1a and 4a) are all associated with the shale fields close to the dark phyllite and one glaucophanite compositions. Provenance discrimination diagrams (Figure 4b) show that most metasedimentary lithologies and two glaucophanites plot in the quartzose and felsic provenance fields, while three glaucophanites and most arc-derived trench-filling sediments reported by Jacques (2013) correlate with the intermediate igneous

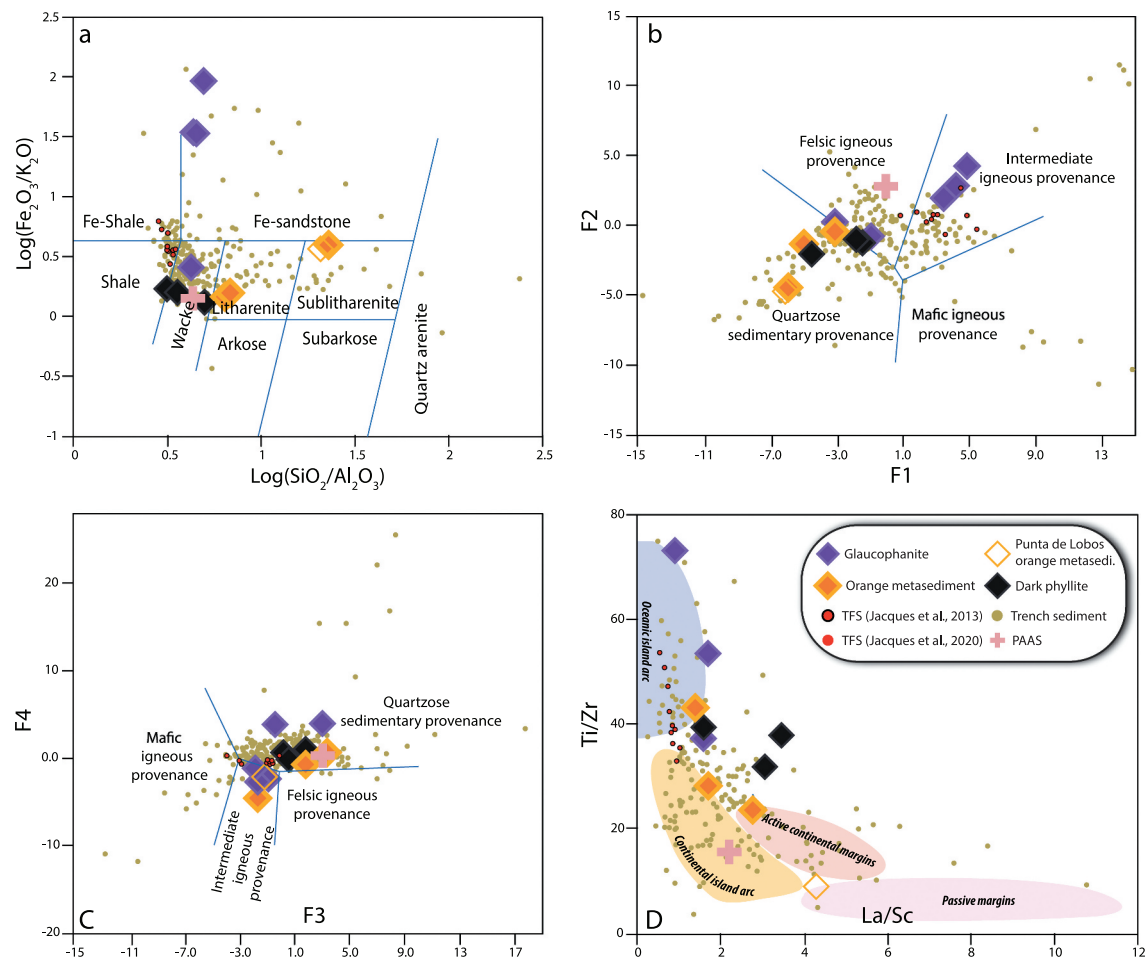


Figure 4. (a) Classification diagram for sedimentary-derived materials (after Herron 1988). (b) and (c) Ratio discrimination diagrams of function 1 ($F1 = -1.773 \cdot \text{TiO}_2 + 0.607 \cdot \text{Al}_2\text{O}_3 + 0.760 \cdot \text{Fe}_2\text{O}_3 \text{ total} - 1.500 \cdot \text{mgo} + 0.616 \cdot \text{cao} + 0.509 \cdot \text{Na}_2\text{O} - 1.224 \cdot \text{K}_2\text{O} - 9.090$) versus function 2 ($F2 = 0.445 \cdot \text{TiO}_2 + 0.070 \cdot \text{Al}_2\text{O}_3 - 0.250 \cdot \text{Fe}_2\text{O}_3 \text{ total} - 1.142 \cdot \text{mgo} + 0.438 \cdot \text{cao} + 1.475 \cdot \text{Na}_2\text{O} + 1.426 \cdot \text{K}_2\text{O} - 6.861$) and function 3 ($F3 = 30.638 \cdot \text{TiO}_2 / \text{Al}_2\text{O}_3 - 12.541 \cdot \text{Fe}_2\text{O}_3 \text{ t} / \text{Al}_2\text{O}_3 + 7.329 \cdot \text{MgO} / \text{Al}_2\text{O}_3 + 12.031 \cdot \text{Na}_2\text{O} / \text{Al}_2\text{O}_3 + 35.402 \cdot \text{K}_2\text{O} / \text{Al}_2\text{O}_3 - 6.382$) versus function 4 ($F4 = 56.500 \cdot \text{TiO}_2 / \text{Al}_2\text{O}_3 - 10.879 \cdot \text{Fe}_2\text{O}_3 \text{ t} / \text{Al}_2\text{O}_3 + 30.875 \cdot \text{MgO} / \text{Al}_2\text{O}_3 - 5.404 \cdot \text{Na}_2\text{O} / \text{Al}_2\text{O}_3 + 11.112 \cdot \text{K}_2\text{O} / \text{Al}_2\text{O}_3 - 3.890$), respectively (after Roser and Korsch 1988). Major oxides are in wt% and normalized as volatile-free (considering the loss of ignition as the total volatile amount). (d) Trace element-based tectonic discrimination diagram after 1986). Details regarding compiled data are given in the caption of the Figure 5. Metasedi.–metasediment.

provenance field. The diagram from Figure 4c shows that most metasedimentary and glaucophanite lithologies are closely associated with the quartzose sedimentary or intermediate provenance fields.

Regarding trace element patterns, the spider diagram from Figure 5a shows that glaucophanites are markedly depleted in Large Ion Lithophile Elements (LILEs) including Sr, while Pb is strongly enriched compared to the blue-green schists. Overall, the trace element pattern of glaucophanites is comparable to those of the other metasedimentary material, except by the strong depletion in K which is evident in the former and explained by the very low abundance of white mica. All our studied lithologies show trace element abundances comparable to the Post Archean Australian Shale standard (PAAS; Taylor and McLennan 1995; updated 2001). On the

other hand, trench sediments collected seaward of Pichilemu and Valparaíso (Jacques *et al.* 2020; Figure 1a) follow in good agreement with the PAAS trend. The main differences are the strong Pb and Sr depletions observed in the blue-green schists and metasedimentary lithologies including glaucophanites, respectively.

Immobile trace element ratios are useful to discriminate between subduction- and non-subduction affinities (Pearce 2008). Th/Yb versus Nb/Yb values in metasedimentary rocks and glaucophanites are strikingly similar, being comparable to compiled trench-filling sediments included those dredged offshore Pichilemu and southernmost regions (Figure 5b). The diagram from Figure 5b shows that all studied lithologies and sedimentary compiled materials fall in the trench-filling sediments trend while OIB compositions from elsewhere and the blue-

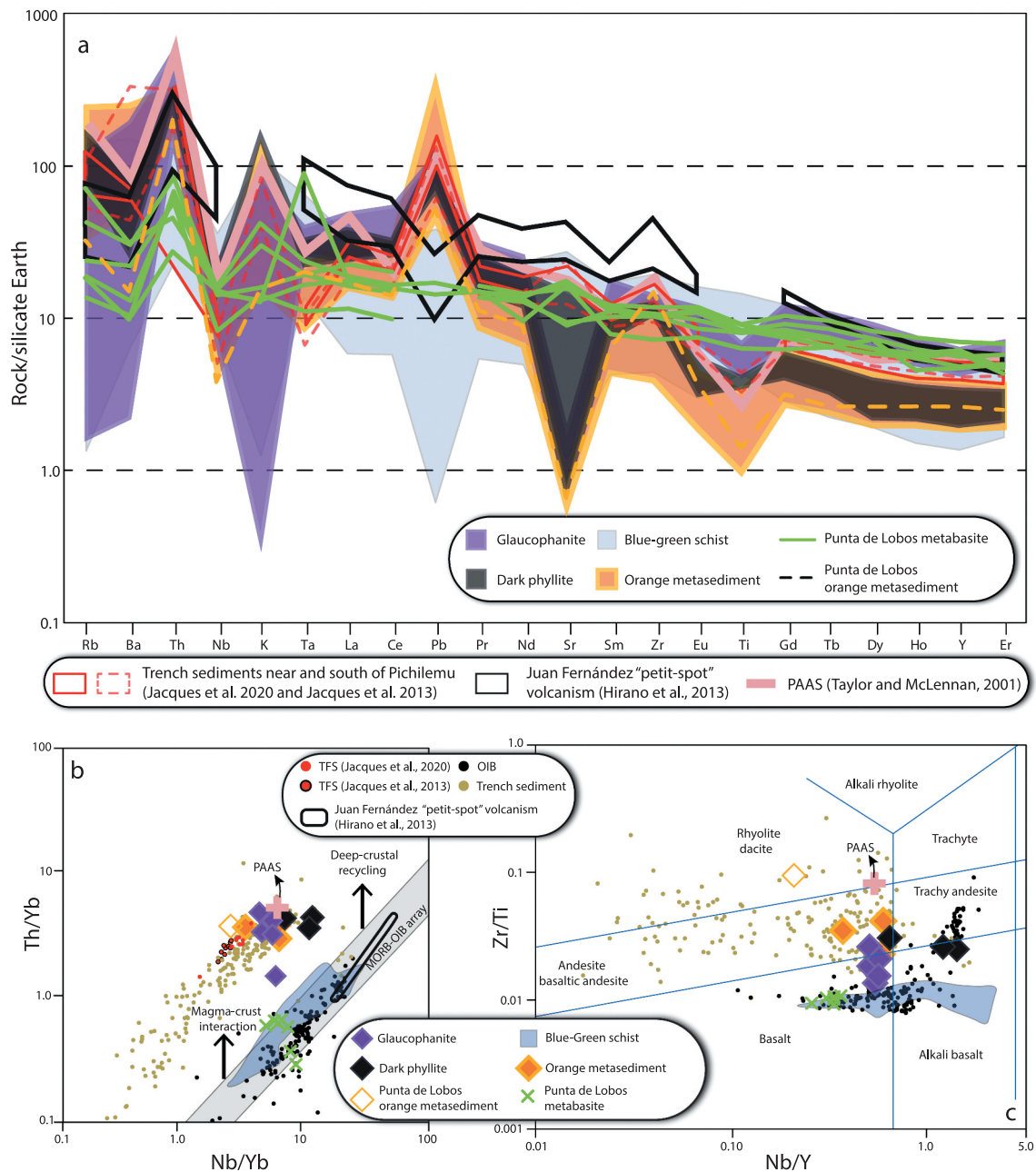


Figure 5. (a) Spider diagram for trace element compositions for all lithologies exposed at Infernillo normalized to the silicate earth standard from McDonough and Sun (1995). (b) Th/Yb versus Nb/Yb diagram (Pearce 2008); note that all blue-green schists analyses fall within the MORB-OIB array while the glaucophanites, orange metasediments and dark phyllites, as well as other trench-filling sediments contain considerably higher Th/Tb ratios. (c) Zr/Ti versus Nb/Y diagram from Winchester and Floyd (1977; modified from Pearce 1996) for all studied lithologies. The glaucophanites and studied metasedimentary rocks together with most trench-filling sediments plot towards andesitic fields. In all diagrams, the blue-green schist compositions correspond to analyses reported in Hyppolito *et al.* (2014), Halama and Konrad-Scholke (2015) and Muñoz-Montecinos *et al.* (2020) while four Punta de Lobos metabasite compositions are from Hyppolito *et al.* (2014). For comparison, trench filling sediments near and south of Pichilemu (Lucassen *et al.* 2010; Jacques 2013; Jacques *et al.* 2020, respectively) and elsewhere including the GLOSS-II compilation from Plank (2014) are shown (Vervoort *et al.* 2011). OIB compositions, mostly from Galapagos and Hawaii have been compiled from the GeoReM dataset (<http://georem.mpch-mainz.gwdg.de/>) together with data from Juan Fernández ridge (central Chile) and 'petit-spot' volcanism (after Hirano *et al.* 2013). PAAS standard composition from Taylor and McLennan (1995/1985; updated in McLennan 2001). The blue-green schist field includes data from 2014), Halama and Konrad-Scholke (2015) and Muñoz-Montecinos *et al.* (2020). The orange metasediments and dark phyllites compositions are from Muñoz-Montecinos *et al.* (2020).

green schists follow the oceanic MORB-OIB array. A similar approach (Figure 5c) demonstrates that the studied metasedimentary and glaucophanite materials plot towards higher Zr/Ti ratios, representing more felsic compositions (without petrogenetic means). Note that most compiled trench-filling sediment compositions are comparable to our studied samples and occupy the same field as in Figure 5(a,b).

Tectonic discrimination diagrams, based on immobile trace element distributions, have been widely used to investigate the nature of sedimentary and metasedimentary materials among different tectonic configurations (see Fuenlabrada *et al.* 2010 for an example). Although the diagrams used here were originally designed for greywackes and sandstones provenance analysis (Bhatia and Crook 1986), for comparison, we have also plotted the glaucophanitic materials. As depicted in Figures 4d and 6(a-c), most studied samples fall within or near the fields representing active oceanic and continental arcs, respectively. Similarly, most trench-filling sediments from elsewhere are also associated with the oceanic and continental arc fields. Trench-filling sediments dredged trench-ward of the Pichilemu region display compositions comparable to those obtained for our studied samples, plotting in the forearc-related fields associated with convergent tectonics (active oceanic and continental arcs).

To better constrain the petrogenesis of the studied lithologies, emphasizing the unknown nature of the glaucophanites, a Al_2O_3 - CaO - FeO - MgO (ACFM) projection was designed using the CSpace software (Torres-Roldan *et al.* 2000); projected from and along the appropriated phases and vectors necessary to condense the compositional space (Figure 7). This projection has been selected as it is commonly used to describe mafic systems (Spear, 1993). Furthermore, by selecting the appropriate

exchange vectors (i.e. KNa_{-1} and $NaSiCa_{-1}Al_{-1}$), the major chemical differences between pelitic compositions can be well appreciated. The exchange vectors have the effect of allowing the concerning elements to exchange identically; thus, for example, a Ca-free phase will be represented as a Ca-bearing phase due to exchange between Na and Si with Ca and Al. Similarly, K, which is an important element in pelitic systems, will also be displayed in the projection due to the selection of the KNa_{-1} exchange vector. In this representation, we have included the trench-filling sediments and OIB volcanics from elsewhere (see caption in Figure 5 for more details) along with the trench-filling sediments dragged from the Chilean subduction trench south of Pichilemu. Our projection shows that the glaucophanites can be correlated to a mineral assemblage (purple tie-triangle in Figure 7) containing major amounts of glaucophane and albite and minor phengite, as observed in the studied samples. Note that due to the selected exchange vector KNa_{-1} , the white mica component is relatively abundant. Nevertheless, such a phase is rare in the natural occurrences. On the other hand, the studied orange metasediments and dark phyllites fall within the grey tie-triangle (Figure 7) defining the albite, phengite and chlorite mineral association. Albite is more abundant in the orange metasediments, in fairly good agreement with the natural occurrences. Finally, the trench-filling sediments from Jacques (2013) are intimately associated with the glaucophanite and orange metasediment compositions representing an intermediate member between the former and the latter.

6. Zircon U-Th-Pb geochronology

SHRIMP U-Th-Pb data is reported in the Supp. Table S2 and the Concordia diagrams in the supplementary

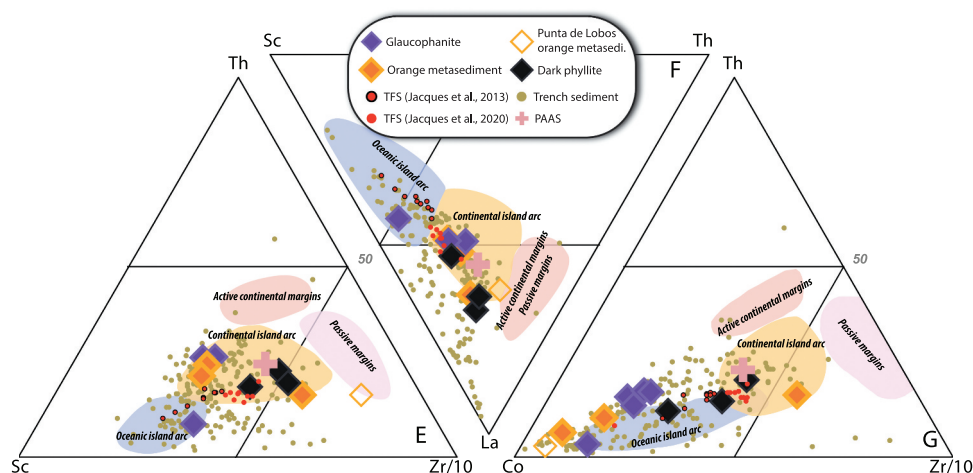


Figure 6. (a) to (c) Trace element-based tectonic discrimination diagrams after 1986). Details regarding compiled data are given in the caption of the Figure 5. Metasedi.–metasediment.

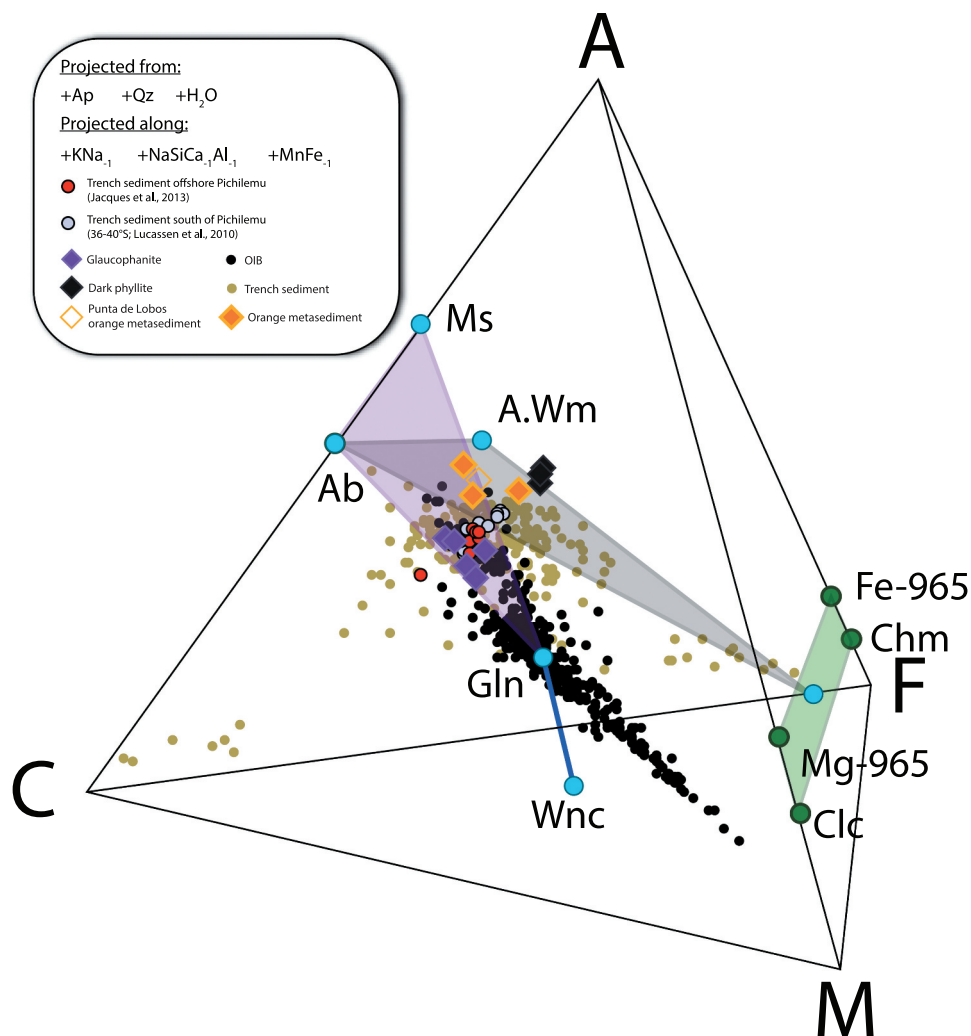


Figure 7. a (Al₂O₃)-C(CaO)-F(FeO)-M(MgO) tetrahedral diagram projected from the phases and exchange vectors as indicated. Fe³⁺ is not considered here for simplicity. The end-members notation is as follow: Ab-Albite; A.Wm – Average white mica from metasedimentary rocks (average composition from seven electron probe microanalyzer data points); Chm – Chamosite; Clc – Clinocllore; Fe-965–chamosite with Fe, Al and Si of 9, 6 and 5 atoms per formula unit; Clc-965–clinocllore with Mg, Al and Si of 9, 6 and 5 atoms per formula unit; Gln – Glaucofanite; Ms – Muscovite; Wnc – Winchite. For information regarding data source see the caption of Figure 5.

Figure S1. For the geochronological results, we consider only data with discordance $< \pm 5\%$. No common Pb contribution was observed, so no Pb-corrections were necessary. Cathodoluminescence images of zircons are displayed in the supplementary material Figure S2.

6.1 Orange metasediments

For sample PI-17-1, 119 grains were analysed, from which 105 were concordant. For sample PI-17-6A we measured 128 crystals and 113 were concordant (Figure S1A and S1B). Zircons from both samples have a wide range of sizes and morphologies and the obtained ages show a comparable and similar distribution Figures 8(a,b). Archaean to

Mesoproterozoic-Ectasian (1203–2654 Ma) ages are scarce, representing c. 9–14% of all analyses. There is an important age population from Mesoproterozoic-Stenian to Neoproterozoic-Tonian (722–1198 Ma) with c. 38–42% of the data and a main cluster at c. 1035 Ma. Neoproterozoic-Cryogenian ages (639–717 Ma) are scarce (c. 4–7% of the data). A significant peak spans Neoproterozoic-Ediacaran to Palaeozoic-Cambrian and Silurian ages (441–635 Ma), comprising c. 25–32% of the data points with a main cluster at c. 523 Ma. The third main cluster corresponds to Palaeozoic-Devonian to Carboniferous ages (313–404 Ma) with a peak at c. 359 Ma (c. 11% of the data). The youngest detrital zircon populations (sedimentation age) in these two samples are virtually identical within error Figures 9(a, b) yielding Carboniferous ages of 336 ± 8 Ma ($n = 4$)

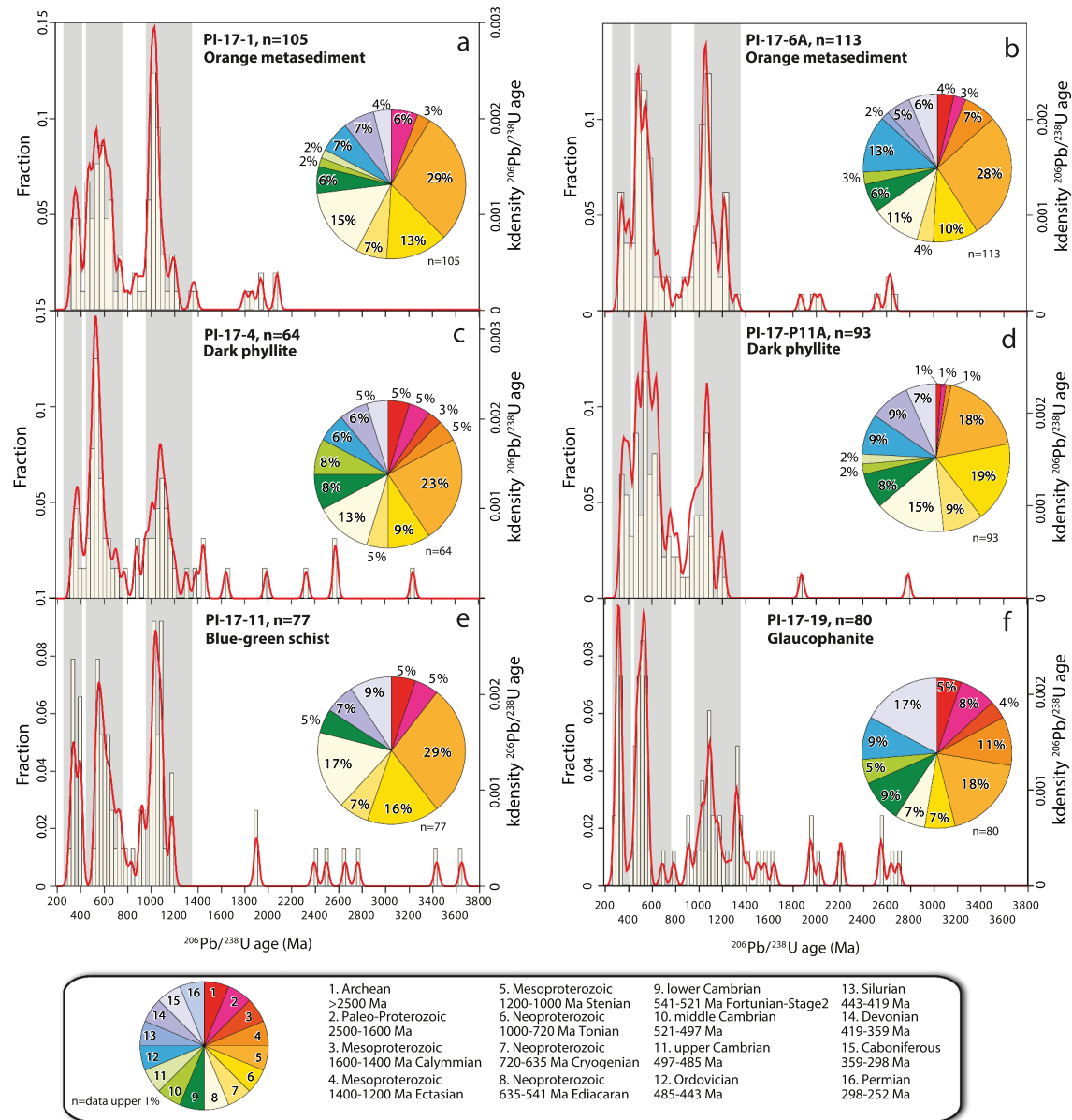


Figure 8. Frequency and density distribution SHRIMP $^{206}\text{Pb}/^{238}\text{U}$ ages diagrams for the orange metasediments (a and b; samples PI-17-1 and PI-17-6A, respectively), dark phyllites (c and d; samples PI-17-4 and PI-17-11A), a greenschist (e; sample PI-17-11) and a glaucophanite (f; sample PI-17-19). To facilitate comparison, all plots include the main zircon age clusters identified in all samples (thick grey vertical band) and pie diagram. The n corresponds to the number zircons analysed.

and 330 ± 7 Ma ($n = 7$) for samples PI-17-1 and PI-17-6A, respectively.

6.2 Dark phyllites

Eighty-four analyses were carried out on the detrital zircon grains from sample PI-17-04, which yielded 64 concordant results. For sample PI-17-11A, we analysed 107 grains, from which 94 were concordant (Figures S1C and S1D). Zircon ages from both samples are statistically comparable, containing identical main zircon clusters

Figure 8(c,d). Archaean to Mesoproterozoic-Ectasian ages (1204–3231 Ma) represent less than c. 9% ($n = 14$) considering both samples. Three detrital zircon age main clusters can be identified in these samples: i) Mesoproterozoic-Stenian to Neoproterozoic-Tonian (742–1192 Ma) with c. 32–37% of the data and a main cluster at c. 1064 Ma; ii) Neoproterozoic-Ediacaran to Palaeozoic-Cambrian to Ordovician ages (452–634 Ma, c. 35–36%) centred at c. 535 Ma; iii) Palaeozoic-Devonian to Carboniferous ages (330–417 Ma) with a main peak at c. 372 Ma (c. 11–16% of the data).

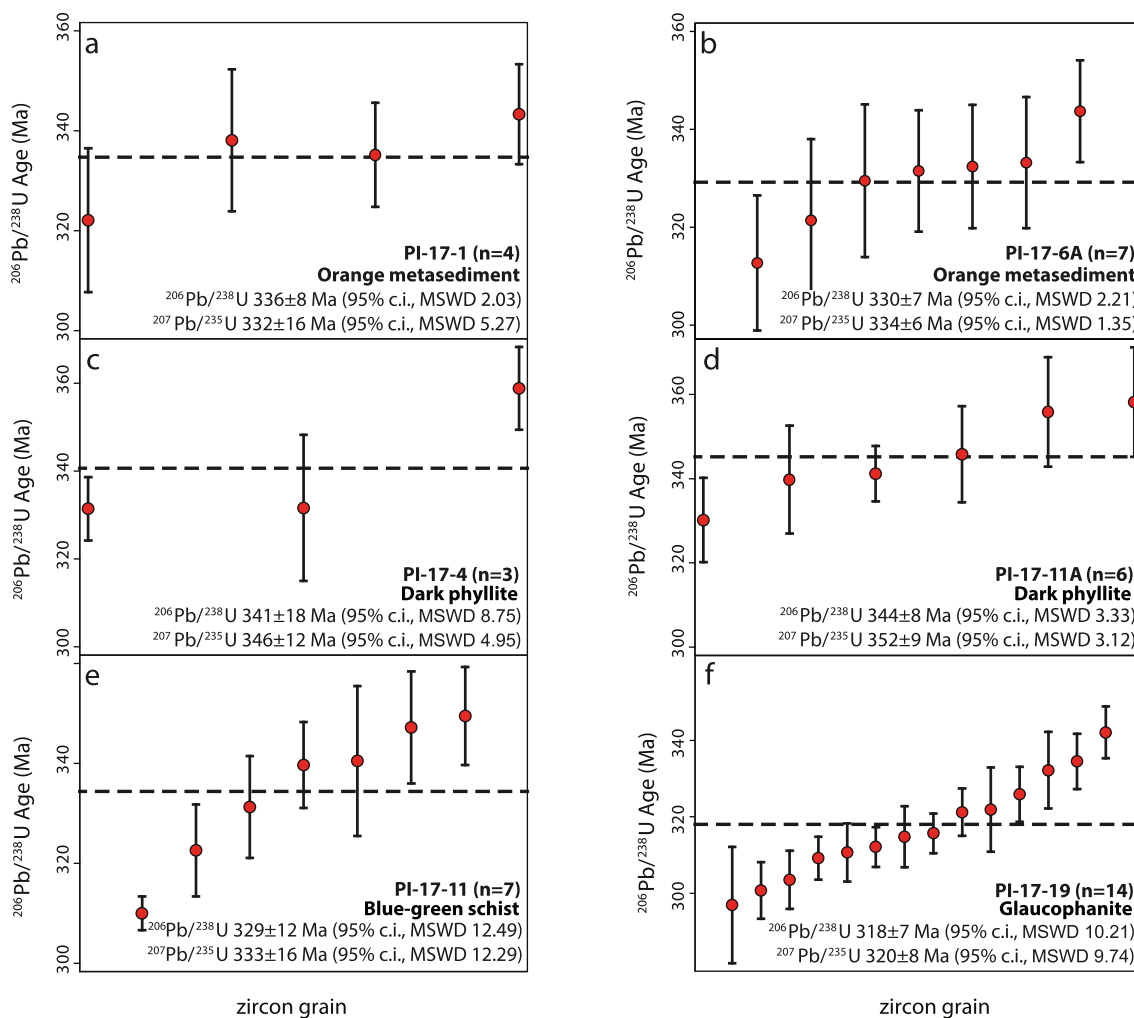


Figure 9. Maximum sedimentation ages for the orange metasediments (a and b; samples PI-17-1 and PI-17-6A, respectively), dark phyllites (c and d; samples PI-17-4 and PI-17-11A), a greenschist (E; sample PI-17-11) and a glaucophanite (F; sample PI-17-19). The maximum sedimentation age was obtained considering the youngest zircon population within analytical error. The $^{206}\text{Pb}/^{238}\text{U}$ and $^{207}\text{Pb}/^{235}\text{U}$ weighted mean and standard deviation at 95% confidence interval (c.i.) are indicated.

Neoproterozoic-Cryogenian ages (639–717 Ma) are scarce, representing c. 7% ($n = 11$) for both samples. The youngest detrital zircon population includes three data points for the sample PI-17-04, with a weighted mean of 341 ± 18 Ma, and six analyses for the sample PI-17-11A, with a weighted mean of 344 ± 8 Ma (Figure 9 (c,d)).

6.3 Blue-green schists

The greenschist sample PI-17-11 contains abundant zircon grains with widths, sizes and morphologies as would be expected in a detrital material. A total of 93 grains were analysed giving 77 concordant results (Figure S1E). Ten per cent of the data corresponds to Archaean to Paleoproterozoic (1897–3648 Ma) ages (Figure 8e). The main population corresponds to Mesoproterozoic-

Stenian to Neoproterozoic-Tonian (722–1182 Ma), which represents c. 45% of the data centred at c. 1053 Ma. There is an important age population from Neoproterozoic-Tonian to Palaeozoic-lower Cambrian ages (524–697 Ma; c. 30% of the data) centred at c. 593 Ma. Last, a third main age population comprises Palaeozoic-Devonian to Carboniferous ages (310–399 Ma), with a peak at c. 360 Ma (c. 28% of the data). The youngest zircon population from this cluster yields a maximum sedimentation age of 329 ± 12 Ma ($n = 7$; Figure 9e).

6.4 Glaucophanite

Surprisingly, the glaucophanite sample (PI-17-19) contains abundant zircon grains relative to the small amount of crushed material (<300 g), with a wide range of sizes and very heterogeneous morphologies

(Figure S2). For this sample, we measured 95 spots, of which 80 resulted in concordant age results (Figure S1F). Archean to Mesoproterozoic-Ectasian (1206–2697 Ma) ages are more abundant than in previous samples (c. 17% of all data), with a main cluster at c. 1318 Ma (Figure 8f). Mesoproterozoic-Stenian to Neoproterozoic-Tonian (782–1165 Ma) ages represent c. 25% of the data centred at c. 1089 Ma. A significant peak (c. 40%) comprises Neoproterozoic-Ediacaran to Palaeozoic-Cambrian and Ordovician ages (441–635 Ma), with a main cluster at c. 512 Ma. Finally, the third main age cluster comprises Palaeozoic Carboniferous ages (297–342 Ma) with c. 15% of the data (Figure 8f), yielding a maximum sedimentation age of 318 ± 7 Ma ($n = 14$) (Figure 9f).

7. Discussion

7.1 On the origin of the materials forming the Infiernillo and Punta de Lobos sequences

7.1.1 Paleo-geographic considerations

Our SHRIMP Zircon U-Pb have age distributions grouped into three main clusters (Figure 10A): i) Mesoproterozoic-Stenian to Neoproterozoic-Tonian (722–1198 Ma, $n = 193$; c. 37% of the data); ii) Neoproterozoic-Ediacaran to Palaeozoic-Cambrian to Devonian ages (359–634 Ma, $n = 202$; c. 38% of the data); iii) Palaeozoic Carboniferous ages (297–359 Ma, $n = 41$; c. 8% of the data). Furthermore, it is possible to recognize, although scarcely and widespread, significant Archaean to Mesoproterozoic-Ectasian contributions (1203–3648 Ma, $n = 67$ c. 11% of the data; Figure 10a). These zircon age populations from Infiernillo virtually match with those clusters reported for other localities belonging to the Western Series (Figure 10b; 34–38°30'S according to Hervé *et al.* 2013). Overall, this detrital signature has been attributed to provenances from the Grenvillian, Pampean and Famatinian orogenic belts located eastward to central East of Argentina (Figure 10; e.g. Charrier *et al.* 2007; Hervé *et al.* 2013; Rapela *et al.* 2016; Rapalini *et al.* 2018). The Proterozoic and Archaean ages may have sourced from reworked materials east of Pichilemu linked to the Transamazonian orogeny, the latter is recognized in the Río de la Plata Craton east of the Sierras Pampeanas in Argentina (Rapela 2007; Figure 10). Note that the craton is considered as a detrital source for metasedimentary sequences (e.g. Sierra de Famatina) since the Upper Cambrian (Verdecchia *et al.* 2011). Compared with other regions of the Palaeozoic accretionary complex of south-central Chile, the studied rocks have zircon age distributions similar to the Eastern series (Willner *et al.*, 2008), even though the main Carboniferous population misses in the latter (Figure

10c). Conversely, the younger Devonian and Carboniferous age populations are more abundant in the southern sector of the Western Series than in Pichilemu and the northern Western Series (Figure 10d).

Maximum deposition ages obtained for the orange metasediments and dark phyllites are in the range of 344 ± 8 to 330 ± 7 Ma, whereas those for the blue-green schists samples are younger, ranging from 329 ± 12 Ma for a greenschist, to 318 ± 7 Ma for a glaucophanite (Figure 9). The main Carboniferous population age cluster is matching with the Carboniferous main population from the Western Series northern Western Series lithologies, which also provide a main maximum sedimentation age range of 307–335 Ma (Figures 1a, 10(a,b); Hervé *et al.* 2013). Note that the maximum sedimentation ages reported here are in the same range as those documented in subduction-related granitoids and the Eastern Series that constituted the Carboniferous volcanic arc and forearc (Willner *et al.* 2005; Hervé *et al.* 2013; Figures 1a and 10). As such, we conclude that all lithologies exposed at Infiernillo, in line with other deposition ages in the region, point to a marked forearc-arc signature (e.g. Willner *et al.* 2005; Hervé *et al.* 2013), indicating effective recycling of continental material coevally with arc activity and forearc erosion (e.g. Eastern Series; see Creixell 2016; Žák *et al.* 2020 for further examples). The maximum sedimentation age from the glaucophanite (318 ± 7 Ma) is close to the peak metamorphism at 292–308 Ma recorded in the region (Willner *et al.* 2005; Hyppolito 2014). Therefore, it is reasonable to conclude that this age marks the end of the sedimentation for Infiernillo lithologies and their incorporation into the subduction channel.

7.1.2 Insights into the provenance and pre-subduction volcano-sedimentary processes

One apparently oceanic-derived sample (PI-17-11, blue-green schist) contains detrital zircons, yielding a maximum sedimentation age of 329 ± 12 Ma. Its protolith is an altered basaltic metatuffaceous material and due to its dominant OIB tholeiitic signature, a continental origin is unlikely (Hyppolito *et al.* 2014 see also Muñoz-Montecinos *et al.* 2020). We interpret this age as representing ancient oceanic volcanic activity and subsequent reworking and continent-derived zircon input along the Gondwana active margin just prior to burial within the subduction channel. These volcanic rocks would not be related to typical mid ocean and/or plume-induced volcanism that formed the oceanic crust as documented in Punta Sirena (Hyppolito *et al.* 2014). Our preferred hypothesis is a 'petit-spot' volcanism (Hirano 2006), which is characterized by younger volcanic activity relative to the oceanic crust it lies on

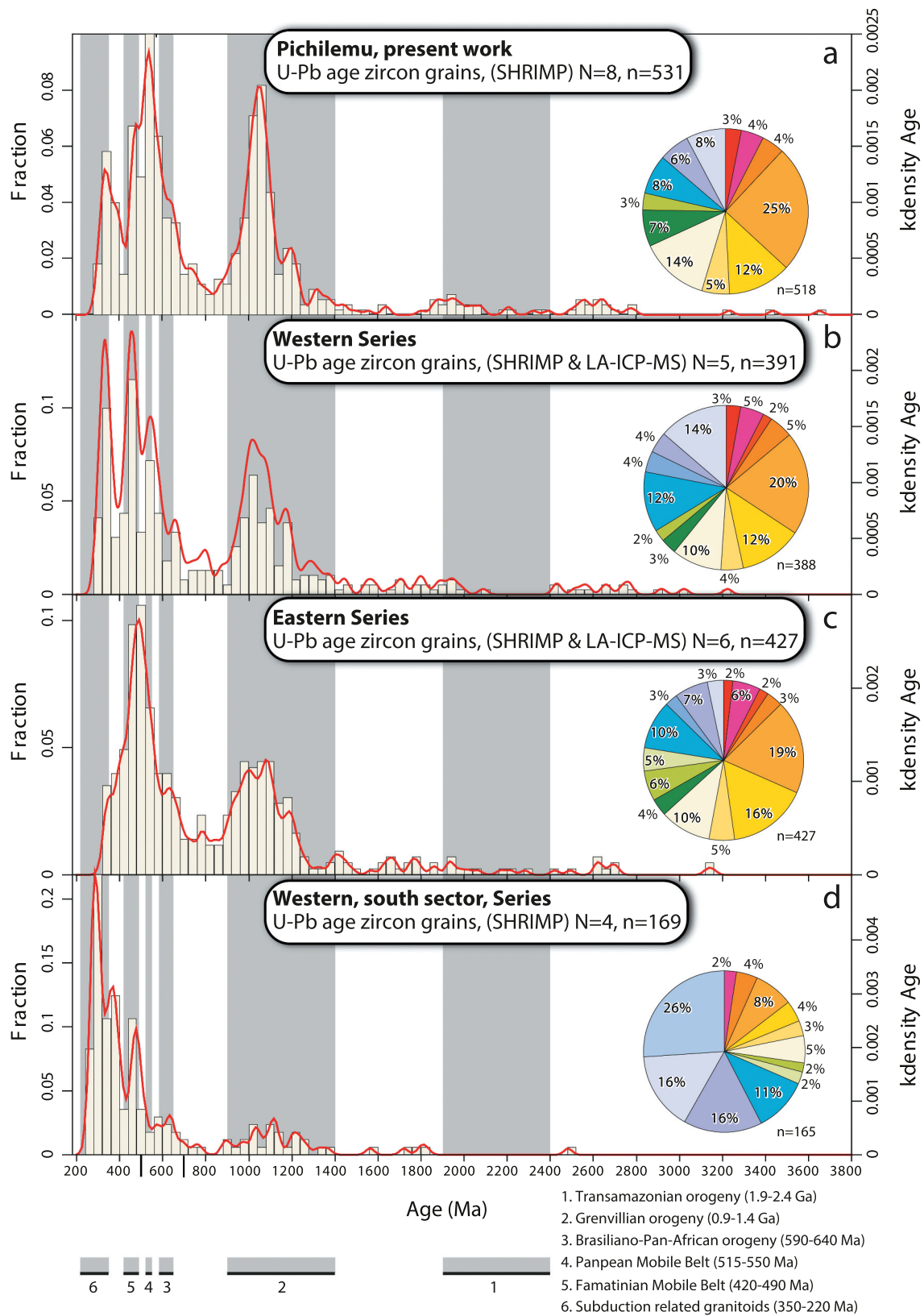


Figure 10. Frequency and density distribution of U-Pb SHRIMP zircon ages diagrams. (a) Samples from Infernillo, Pichilemu region (this work). (b) Western Series of Central Chile (north sector). (c) Eastern Series of Central Chile. (d) Western Series of Central South-Chile. Compiled zircon U-Pb ages are from Willner et al. (2008) and Hervé et al. (2013), see also Casquet et al. (2018). To facilitate comparison, vertical bands indicating main orogenic events identified in East Argentina and Central Chile are displayed in all plots. Pie diagram as in Figure 8. N—number of individual samples; n—zircon point ages.

and is produced due to fracturing near the outer rise induced by plate flexure during subduction. For example, young (up to 10 Ma) volcanoes have been recently discovered on the Cretaceous Pacific and Palaeogene Nazca Plates that subduct beneath Japan and central Chile (e.g. part of the Juan Fernandez Ridge), respectively (Hirano 2011; Hirano *et al.* 2013), and have been characterized as OIB-like materials (Hirano 2006; Yamamoto *et al.* 2020).

The trace element patterns of fresh 'petit spot' lavas in the Juan Fernandez ridge system are slightly richer in the trace element abundances compared to Infiernillo-Punta de Lobos metavolcanics (Figure 5a; Hirano *et al.* 2013). Nevertheless, their patterns are similar: LILEs are relatively depleted, Th and Pb show important positive and negative anomalies, respectively, while LREEs abundances are higher than HREEs with a systematic decrease towards the latter. In addition, the apparent small-scale dimensions (likely less than 10 km²) of the Punta de Lobos metapillow lavas support a scenario where low-volume volcanic products formed the massif, as proposed for other accretionary settings in the Pacific margin and elsewhere (Buchs *et al.* 2013; Yang *et al.* 2015). However, a link between the investigated OIB-like products and a plume-derived origin cannot be ruled out (Yamamoto *et al.* 2020). Under this perspective, the Punta de Lobos massif might represent a small, scrapped section of a former larger-scale subducted seamount (e.g. Hervé *et al.* 1994; Bonnet *et al.* 2019, 2020). It seems clear that the blue-green schists from Infiernillo-Punta de Lobos complex do not represent typical mid ocean ridge products as further south (e.g. Hyppolito *et al.* 2014). Unfortunately, the precise nature of these metavolcanic lithologies is still poorly constrained. Further isotopic and geophysical studies (e.g. Sanhueza *et al.* 2021) might provide novel constraints on the origin and dimensions of the volcanic massif.

Trace element patterns show that all metasedimentary and glaucophanitic lithologies exposed in the Infiernillo-Punta de Lobos sequence, as well as trench-filling sediments dredged offshore Pichilemu region are comparable (Figure 5a). The Pb peak, which is characteristic of continent-derived materials (e.g. Plank 2014), is present in all lithologies except in the blue-green schists. The low abundance of Rb, Ba and K in the glaucophanites is explained by the lack of phengite: a well-known carrier for LILEs. Negative Sr anomalies displayed in the studied metasedimentary rocks and glaucophanites, while absent in the trench-filling sediments and PAAS, are more difficult to reconcile. In a similar way as Eu, Sr²⁺ is preferentially partitioned into phases containing Ca²⁺

such as plagioclase, representing thus an inherited feature from the volcanic, arc-related protoliths (e.g. McLennan and Taylor 1991). However, fluid-rock interactions during subduction may also redistribute Sr (e.g. Muñoz-Montecinos *et al.* 2021). Th/Yb vs. Nb/Yb and Zr/Ti vs. Nb/Y ratios Figure 5(b,c) show that the studied lithologies can be subdivided into two groups: the blue-green schists, which is related to the OIB array (e.g. Hyppolito *et al.* 2014), and the trench-filling sediments array. In the latter, our investigated lithologies, the PAAS standard as well as the compilation of trench-filling sediments, including localities offshore Pichilemu have virtually identical immobile trace element ratios, pointing to a homogeneous provenance.

Provenance discrimination diagrams show that all the metasedimentary material (orange metasediments and dark phyllites) plots within the quartzose sedimentary provenance, closely associated with the glaucophanite compositions Figure 4(b,c). Although three glaucophanite compositions fall within the intermediate igneous provenance field. The ACFM projection (Figure 7) depicts that the glaucophanite samples correlate well with compositions from trench-filling sediments (near Pichilemu and elsewhere) as well as with some Al-rich, OIB compositions. The orange metasediments are also associated with the trench-filling sediments but not with OIB compositions. Therefore, based on zircon U-Pb isotopic analyses, major and trace elements investigations as well as geological constraints, we conclude that most metasedimentary material along with the glaucophanites forming the metamorphic basement at Infiernillo-Punta de Lobos locality share a common Carboniferous origin.

Ti-Zr-La-Sc-Th-Co systematics (Figure 6(a-c)) show that all studied lithologies correlate well with the fields associated with oceanic and/or continental arc settings, possibly in a forearc region (Bhatia and Crook 1986). Remarkably, present-day trench-filling sediments from elsewhere and near Pichilemu are also intimately associated with the oceanic and continental fields from Figure 6(a-c). In this case, however, the deposition and provenance environments are well known and occurred in the trench, as continent-derived materials supplied by the erosion of the Cretaceous to Holocene Andean arc (Völker *et al.* 2008; Lucassen *et al.* 2010; Jacques 2013). We conclude that all studied metasedimentary and possibly glaucophanitic materials at Infiernillo correspond to former trench-filling deposits with a forearc-arc signature deposited near the paleo-trench of the active continental margin of Gondwana at c. 344–318 Ma (see also Willner *et al.* 2005; Agard *et al.* 2009; Plank 2014; Buchs and Oemering 2020).

For the glaucophanites, fine-scale layering within blue-green schists suggests alternances (and intermit- tences) between sedimentary-volcanic processes. Several hypotheses could be invoked to explain glaucophanite occurrence peculiarity: (1) erosion of the OIB-like oceanic relief and further mixing with continent-derived sediments and deposition on its flanks; (2) intermit- tences of arc-derived pyroclastic flows that reached the trench at a maximum age of 318 ± 7 Ma; (3) forearc-derived gravitational mass flow sediments finely inter- leaved within reworked oceanic materials. The first and second hypotheses are partially supported by the find- ing of rare hornblende cores, likely pointing to a volca- nic or a seafloor-derived hydrothermal source (Hyppolito 2014; Muñoz-Montecinos *et al.* 2020). In addition, major and trace element signatures of the glaucophanites reveal a strong (or highly evolved) crustal component, indicating a continent-derived origin (options 2 and 3). It has been speculated that the glaucophanites represent metasomatized domains during subduction (Halama and Konrad-Schmolke 2015). However, several evi- dences, such as extremely sharp contacts with the sur- rounding lithologies, lack of alteration selvages, preservation of fresh oceanic signatures in adjacent host blueschists and greenschists, among others, point to a bulk lithological control rather than selective meta- somatism (Muñoz-Montecinos *et al.* 2020; see Hernández-Urbe *et al.* 2020 for further examples). We conclude that recurrent continent-derived pyroclastic flows or sedimentary (possibly volcanoclastic) mass transport deposits (options 2 and 3) represent the best candidates to account for the formation of glaucopha- nite layers within the Infiernillo-Punta de Lobos complex (see Noda and Sato 2018; Aoki 2014 for similar inferences).

Last, the overlap of RSCM temperatures at around 400°C confirms that the dark phyllites slivers from Infiernillo reached virtually identical peak meta- morphic conditions, in line with Muñoz-Montecinos *et al.* (2020) who considered all Infiernillo exposures as a cofacial metamorphic sequence. We thus stress the importance of the Infiernillo-Punta de Lobos sequence, which almost continuously exposes one of the few circum-Pacific examples where a relatively coherent forearc-arc-derived metamorphic pile (along with minor oceanic-derived slivers) can be documen- ted. This ensemble was substantially affected by nearly coaxial basal accretion deformation followed by further deep duplex exhumation across the forearc crust (Willner *et al.* 2005). Note that geophysical investigations image a similar stack of lithologies that are currently being accreted to the base of the Cascadia forearc (Delph *et al.* 2021).

7.2 Subduction of continent-derived and trench- filling sediments towards HP conditions

Underplating of thick mafic sequences, some of which possibly representing oceanic roughness, as well as related sediments has been proven to actively occur at depths down to 45 km (e.g. Uchida *et al.* 2010; Ramos *et al.* 2018; Scholl 2019). Our field, geochemical and geo- chronological investigations demonstrate that conti- nent-derived metasedimentary and massive oceanic materials were coevally and coherently subducted and accreted at transitional blueschist-facies conditions. We postulate, based on previous experimental and numer- ical results (Lallemand *et al.* 1994; Ruh *et al.* 2016; Noda *et al.* 2020), that this scenario may have been possible thanks to the entrance of the Punta de Lobos edifice as a subducted stiff oceanic relief. While the rest of the Infiernillo-Punta de Lobos sequence corresponds to the metavolcanosedimentary materials deposited in the trench and in the surroundings of the oceanic high (Figure 11a; e.g. Noda *et al.* 2020). Once the Punta de Lobos oceanic relief started subducting, the subduction channel widened allowing transfer of trench sediments beyond the frontal accretionary and shallow underplat- ing regions (Figure 11b). This allowed the décollement to be positioned on the flanks above the oceanic relief, causing uplift of the overriding forearc (Dominguez *et al.* 2000; Raimbourg *et al.* 2014; Noda *et al.* 2020). A similar process has been invoked in the South Shetland Islands (Antarctica), where a potentially subducted seamount induced accretion and further exhumation of the mate- rials buried down to c. 25 km depth (Trouw *et al.* 1998). This mechanism is strongly dependent on the stiffness or strength of the subducting oceanic high, which is ulti- mately affected (i.e. weakened) by variations in pore fluid pressures (Moreno 2018; Menant *et al.* 2019; Sun *et al.* 2020).

Up to date, few cases of subducted, now-exhumed seamounts have been reported in the geological record (e.g. Wilson *et al.* 1989; Hervé *et al.* 1994; John *et al.* 2010). One of the best characterized field examples has been documented by Bonnet *et al.* (2020 and Bonnet *et al.* 2020; see also Angiboust *et al.* 2016 for information on the geological context), and corresponds to the fully exposed Siah-Kuh seamount in Southeastern Iran. This massif is c. 1.5 km-high and has been apparently com- pletely sheared off, with few traces of paleo-seismicity (Bonnet *et al.* 2019). In our study locality, the exposed section of the Punta de Lobos massif is a few hundreds of metres-thick at most if considering its southernmost prolongation (Figure 1b). We note that these dimensions might be underestimated owing to the effect of recent Quaternary marine erosion well visible along the

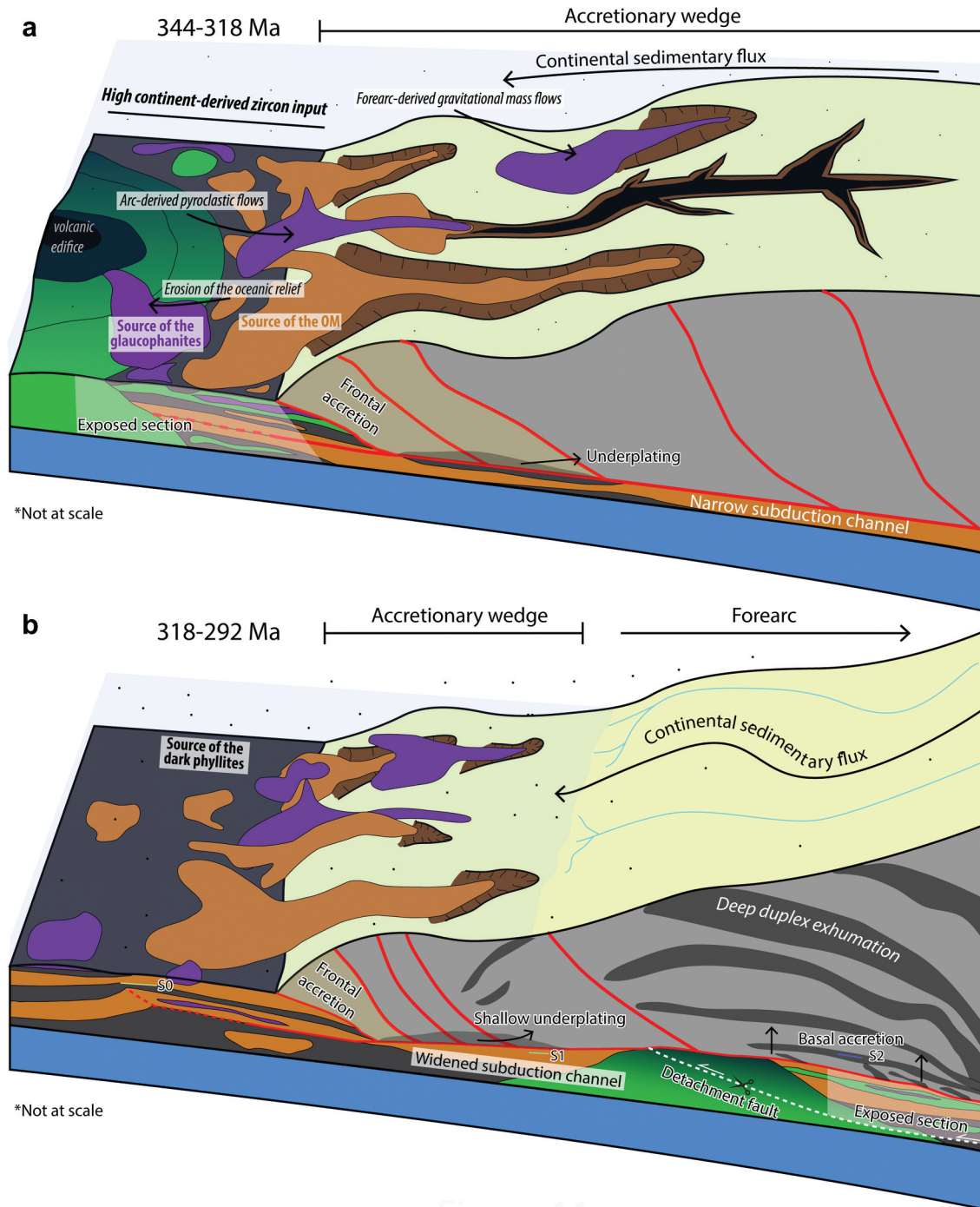


Figure 11

Figure 11. Simplified subduction zone sketches illustrating different snapshots of sedimentary, tectonic and metamorphic processes of Infiernillo-Punta de Lobos sequences. (a) Early depositional stages of former Infiernillo-Punta de Lobos metasedimentary and glaucophanitic materials, associated with gravity-induced mass transport towards the trench allowing interlayering with former pelagic dark phyllites and oceanic materials. The green body represents the Punta de Lobos massif approaching the trench. Sedimentary reworking of this oceanic high allowed the formation of slope deposits identical in composition but with a strong continental signature of zircon ages (e.g. greenschist sample PI-17-11); note that at this stage (e.g. before oceanic high subduction), frontal accretion enhances the growth of the accretionary wedge narrowing the subduction channel. (b) Later, subduction-related HP-LT metamorphic stage affecting the Infiernillo-Punta de Lobos complex. In this phase, the entrance of the Punta de Lobos massif widened the subduction channel allowing the metasedimentary and glaucophanitic materials nearby to subduct. At peak conditions, the oceanic roughness cannot withstand the increasing shear forces applied on the uppermost part of the seamount, which ultimately leads to underthrusting and basal accretion along with the surrounding material. After detachment, all the Infiernillo-Punta de Lobos material started exhumation via nappe-stacking and deep duplex formation. The ages shown in panel a correspond to the maximum sedimentation ages obtained in this study, while those shown in panel B are the youngest maximum sedimentation age obtained for the glaucophanite and the peak metamorphic stage given by Willner *et al.* (2005). The deep duplex exhumation sketch from panel B has been depicted according to Menant *et al.* (2019).

erosional terraces overlaying the massif (e.g. Figures 2b and 3f). However, its mechanical strength must have been strong enough to support progressively increasing shear stresses up to c. 25 km depths at the base of the seismogenic zone, before detachment from the subducting slab (e.g. Agard *et al.* 2018). Few metapillow lava massifs analogues to the one exposed in Punta de Lobos have been recognized in Chile to the best of our knowledge, while several metapillow lava bodies (some of them with OIB signatures) have been described further south along the Western Series (e.g. Punta Sirena: Hyppolito *et al.* 2014 Los Pabilos: Kato *et al.* 2008). Indeed, in Chilean Antarctica, Wilson *et al.* (1989; see also Davidson *et al.* 1989) described the occurrence of blueschist-facies metabasalts, metapillow lavas-brecias and a phyllite-rich mélange interpreted as a former subducted seamount basally accreted to the Gondwana continent during Jurassic times. Interestingly, the authors also report cataclastic shear bands, penetrative brittle structures and boudinage that are inferred to have occurred during prograde burial, underplating and further exhumation. Overall, it is not surprising to expect seamount fragments here and there in the entire Chilean-Antarctic paleo-accretionary system given (i) the extremely long duration of basal accretion processes that have led to the formation of this complex (several tens of Myr; Willner *et al.* 2005; Hyppolito *et al.* 2014; Calderón *et al.* 2016; Angiboust *et al.* 2018) and (ii) the relatively high abundance of seamounts in the present-day Pacific basin which may be considered as a good analogue for the Carboniferous Proto-pacific seafloor.

Even though our Raman thermometric results together with observed mineral parageneses indicate sensibly similar peak burial conditions for all the material forming the Infernillo-Punta de Lobos rocks, it is still challenging to specify where the decapitation or detachment of the oceanic high and metasedimentary materials occurred. Numerical modelling suggests that most of the shearing and tectonic mixing occurring during subduction take place through peak basal accretion and not upon exhumation (Menant *et al.* 2019; Angiboust *et al.* 2022), as high-strain fabrics are expected and observed in the former case (e.g. Glodny *et al.* 2005; Richter *et al.* 2007; Ring, 2008; Platt *et al.* 2018). Note though that mixing of minor amplitude is possible along later strike-slip structures (Kato and Godoy 2015). Our field observations, namely the occurrence of (i) prograde-related foliations (i.e. S1), (ii) former extensional veins transposed to a pervasive main foliation S2 (Muñoz-Montecinos *et al.* 2020) and (iii) highly strained and flattened metapillow lavas, support the scenario where basal accretion produced the maximum amount of strain (Menant *et al.* 2019).

Altogether, these experimental and numerical investigations along with field-based results are key to constrain the factors influencing the mechanical coupling of the plate interface (Cloos and Shreve 1996; Behr and Becker 2018; Agard *et al.* 2018). The effect of subducted oceanic reliefs such as seamounts on megathrust ruptures has been a matter of vivid debate. While some authors propose that subduction of oceanic roughness may promote large earthquakes along the megathrust (asperities; Cloos 1992; Scholz and Small 1997; Bilek *et al.* 2003; Yang *et al.* 2013), others suggest that oceanic highs arrest earthquake propagation, facilitating creep and decoupling (barriers: Wang and Bilek 2011; Geersen *et al.* 2015; Bonnet *et al.* 2020). On the other hand, the presence or absence of subducted sediments has also been thought as a factor controlling earthquake nucleation and magnitude. In this case, these materials are regarded as sources of pore fluids or contact zones of low friction coefficients that can effectively weaken the megathrust, facilitating seismic slip (Ruff 1989; Li 2018; Muldashev and Sobolev 2020). In the Infernillo-Punta de Lobos complex, the exposed subducted sediments are capping the oceanic relief and may represent suitable layers for earthquake nucleation (Heuret *et al.* 2012). Yet, recent studies on the northern part of the Chilean margin have shown that subducted highs arrested further earthquake rupturing along-strike and up-dip of a large megathrust earthquake (Iquique 2014 earthquake, 8.1 Mw; Geersen *et al.* 2015). At the Pichilemu locality, the current state of knowledge does not allow attesting whether the mechanism of plate roughness detachment was seismogenic or not, as no firm evidence of seismic-related structures has been documented (e.g. Rowe *et al.* 2005; Muñoz-Montecinos *et al.* 2021). Thus, further high-resolution investigations along the Western Series and elsewhere are necessary to systematically determine the effects of oceanic roughnesses and sediment subduction in the light of plate interface rheology.

8. Conclusions

In the Pichilemu region, deep-seated remnants of the Carboniferous Chilean paleo-accretionary wedge are exceptionally preserved, illuminating the composition and emplacement dynamics of the plate interface. Our detrital zircon geochronological study demonstrates that all lithologies forming the Infernillo-Punta de Lobos complex document similar maximum deposition ages. In agreement with previous studies, these results suggest that the sediments were sourced in the Palaeozoic Pampean and Famatinian orogens, but most remarkably in the Carboniferous arc and forearc (Hervé *et al.* 2013). Together with petro-geochemical constraints, it is possible

to associate the studied material with sedimentary sources similar to those recorded in present-day trench-filling sediments. It thus suggested that all metasedimentary and glaucophanitic lithologies exposed in the Infernillo-Punta de Lobos sequence represent trench-filling material derived from the Carboniferous arc, as well as remobilization of forearc material. In addition, one ocean-derived metatuff yields similar depositional ages indicating active oceanic volcanism near the trench (e.g. petit-spot volcanism). The fine-scale interlayering of these lithologies points to recurrent sedimentary and/or volcanic-pyroclastic processes occurring over the oceanic material near the trench environment. The close spatial association with the meta-volcanosedimentary lithologies, with an edifice composed of strained metapillow lavas suggests a common metamorphic history for these coherent sequences, which probably reached identical peak conditions as supported by Raman thermometric studies on carbonaceous matter. Our findings are in line with previous experimental and numerical investigations suggesting that the occurrence of metavolcanic edifices is key to allow trench-fill sediment mass transfer far beyond the shallow accretionary wedge region. These results, together with geological constrains (i) allow documenting in detail the physical processes operating at depth in the Chilean paleo-subduction zone, (ii) provide new lights on the effectiveness of crustal recycling processes and (iii) contribute to a better understanding of the mechanical interplay between oceanic highs subduction and thick sedimentary sequences in the deep subduction environment.

Acknowledgments

First of all, we would like to thank Antonio García Casco, to whom this paper is dedicated. Antonio is an extremely supportive and exceptionally passionate person, especially when discussing about geology, jade, and the history of Granada city, always keen to illustrate his ideas on a napkin. We hope that, despite the distance, we will continue sharing beautiful moments and benefiting from his wisdom. The logistical assistance of Mauricio Calderón and the Earth Sciences Department at University Andrés Bello are warmly acknowledged. JMM expresses his gratitude to Francisco Fuentes for discussions regarding volcanic processes and regional Chilean geology as well as to his family for field assistance during the 2020 expedition. T. Hyppolito is acknowledged for insightful discussions at the early stages of this project. The editorial handling by Bob Stern and Yamirka Rojas-Agramonte as well as the insightful comments from John Platt and three anonymous reviewers are very much appreciated. Damien Deldicque (ENS Paris) is also acknowledged for providing access to the Raman spectrometer. Funding for this project has been provided by an IDEX grant 16CR538 to SA. This is IBERSIMS publication n° 104. The authors report there are no competing interests to declare.

Disclosure statement

No potential conflict of interest was reported by the authors.

Funding

The work was supported by the IDEX [6CR538].

ORCID

Jesus Munoz-Montecinos  <http://orcid.org/0000-0002-7719-9463>

Aitor Cambeses  <http://orcid.org/0000-0003-2972-4718>

References

- Agard, P., Plunder, A., Angiboust, S., Bonnet, G., and Ruh, J., 2018, The subduction plate interface: Rock record and mechanical coupling (from long to short timescales). *Lithos*, v. 320, p. 537–566. [10.1016/j.lithos.2018.09.029](https://doi.org/10.1016/j.lithos.2018.09.029)
- Agard, P., Yamato, P., Jolivet, L., and Burov, E. 2009, Exhumation of oceanic blueschists and eclogites in subduction zones: Timing and mechanisms. *Earth-Science Reviews*, v. 92, no. 1–2, p. 53–79. [10.1016/j.earscirev.2008.11.002](https://doi.org/10.1016/j.earscirev.2008.11.002)
- Aguirre, L., Hervé, F., and Godoy, E. 1972, Distribution of metamorphic facies in Chile: An outline. *Krystallinikum*, v. 9, no. 1, p. 7–19.
- Angiboust, S., Agard, P., Glodny, J., Omrani, J., and Oncken, O. 2016, Zagros blueschists: Episodic underplating and long-lived cooling of a subduction zone. *Earth and Planetary Science Letters*, v. 443, p. 48–58. [10.1016/j.epsl.2016.03.017](https://doi.org/10.1016/j.epsl.2016.03.017)
- Angiboust, S., Cambeses, A., Hyppolito, T., Glodny, J., Monié, P., Calderón, M., and Juliani, C. 2018, A 100-my-long window onto mass-flow processes in the Patagonian Mesozoic subduction zone (Diego de Almagro Island, Chile). *Bulletin*, v. 130, no. 9–10, p. 1439–1456. [10.1130/B31891.1](https://doi.org/10.1130/B31891.1)
- Angiboust, S., Hyppolito, T., Glodny, J., Cambeses, A., Garcia-Casco, A., Calderón, M., and Juliani, C. 2017, Hot subduction in the middle Jurassic and partial melting of oceanic crust in Chilean Patagonia. *Gondwana Research*, v. 42, p. 104–125. [10.1016/j.gr.2016.10.007](https://doi.org/10.1016/j.gr.2016.10.007)
- Angiboust, S., Menant, A., Gerya, T., and Oncken, O., 2022, The rise and demise of deep accretionary wedges: A long-term field and numerical modeling perspective. *Geosphere*, v. 18, no. 1, p. 69–103.
- Aoki, K., 2014, Provenance diversification within an arc-trench system induced by batholith development: The Cretaceous Japan case. *Terra Nova*, v. 26, no. 2, p. 139–149. [10.1111/ter.12080](https://doi.org/10.1111/ter.12080)
- Aron, F., Cembrano, J., Allmendinger, R.W., Astudillo, F., and Arancibia, G., 2012 December, Structural geology of the active forearc above the maule megathrust: Traces of a long-lived subduction segment. XIII Chilean geological congress, Antofagasta, Chile, p. 5–9. <https://ui.adsabs.harvard.edu/abs/2012AGUFM.T41E.08A/abstract>
- Bassett, D., and Watts, A.B. 2015, Gravity anomalies, crustal structure, and seismicity at subduction zones: 1. Seafloor roughness and subducting relief. *Geochemistry*,

- Geophysics, Geosystems, v. 16, no. 5, p. 1508–1540. [10.1002/2014GC005684](https://doi.org/10.1002/2014GC005684)
- Behr, W.M., and Becker, T.W. 2018, Sediment control on subduction plate speeds. *Earth and Planetary Science Letters*, v. 502, p. 166–173. [10.1016/j.epsl.2018.08.057](https://doi.org/10.1016/j.epsl.2018.08.057)
- Beysac, O., Goffé, B., Chopin, C., and Rouzaud, J.N. 2002, Raman spectra of carbonaceous material in metasediments: A new geothermometer. *Journal of Metamorphic Geology*, v. 20, no. 9, p. 859–871. [10.1046/j.1525-1314.2002.00408.x](https://doi.org/10.1046/j.1525-1314.2002.00408.x)
- Bhatia, M.R., and Crook, K.A. 1986, Trace element characteristics of graywackes and tectonic setting discrimination of sedimentary basins. *Contributions to Mineralogy and Petrology*, v. 92, no. 2, p. 181–193. [10.1007/BF00375292](https://doi.org/10.1007/BF00375292)
- Bilek, S.L., Schwartz, S.Y., and DeShon, H.R. 2003, Control of seafloor roughness on earthquake rupture behavior. *Geology*, v. 31, no. 5, p. 455–458. [10.1130/0091-7613\(2003\)031<0455:COSROE>2.0.CO;2](https://doi.org/10.1130/0091-7613(2003)031<0455:COSROE>2.0.CO;2)
- Black, L.P., Kamo, S.L., Allen, C.M., Aleinikoff, J.N., Davis, D.W., Korsch, R.J., and Foudoulis, C. 2003, TEMORA 1: A new zircon standard for Phanerozoic U–Pb geochronology. *Chemical Geology*, v. 200, no. 1–2, p. 155–170. [10.1016/S0009-2541\(03\)00165-7](https://doi.org/10.1016/S0009-2541(03)00165-7)
- Bonnet, G., Agard, P., Angiboust, S., Fournier, M., and Omrani, J. 2019, No large earthquakes in fully exposed subducted seamount. *Geology*, v. 47, no. 5, p. 407–410. [10.1130/G45564.1](https://doi.org/10.1130/G45564.1)
- Bonnet, G., Agard, P., Angiboust, S., Monié, P., Fournier, M., Caron, B., and Omrani, J. 2020, Structure and metamorphism of a subducted seamount (Zagros suture, Southern Iran). *Geosphere*, v. 16, no. 1, p. 62–81. [10.1130/GES02134.1](https://doi.org/10.1130/GES02134.1)
- Bonnet, G., Agard, P., Whitechurch, H., Fournier, M., Angiboust, S., Caron, B., and Omrani, J. 2020, Fossil seamount in southeast Zagros records intraoceanic arc to back-arc transition: New constraints for the evolution of the Neotethys. *Gondwana Research*, v. 81, p. 423–444. [10.1016/j.gr.2019.10.019](https://doi.org/10.1016/j.gr.2019.10.019)
- Buchs, D.M., and Oemering, S.A. 2020, Long-term non-erosive nature of the south Costa Rican margin supported by arc-derived sediments accreted in the Osa Mélange. *Earth and Planetary Science Letters*, v. 531, p. 115968. [10.1016/j.epsl.2019.115968](https://doi.org/10.1016/j.epsl.2019.115968)
- Buchs, D.M., Pilet, S., Cosca, M., Flores, K.E., Bandini, A.N., and Baumgartner, P.O. 2013, Low-volume intraplate volcanism in the early/middle Jurassic Pacific basin documented by accreted sequences in Costa Rica. *Geochemistry, Geophysics, Geosystems*, v. 14, no. 5, p. 1552–1568. [10.1002/ggge.20084](https://doi.org/10.1002/ggge.20084)
- Calderón, M., Hervé, F., Fuentes, F., Fosdick, J.C., Sepúlveda, F., and Galaz, G. 2016, Tectonic evolution of Paleozoic and Mesozoic andean metamorphic complexes and the Rocas Verdes ophiolites in southern Patagonia. in Ghiglione, M.C. eds. *Geodynamic Evolution of the Southernmost Andes*, p. 7–36. Springer Earth System Sciences:Cham. [10.1007/978-3-319-39727-6_2](https://doi.org/10.1007/978-3-319-39727-6_2)
- Calvert, A.J., Ramachandran, K., Kao, H., and Fisher, M.A. 2006, Local thickening of the Cascadia forearc crust and the origin of seismic reflectors in the uppermost mantle. *Tectonophysics*, v. 420, no. 1–2, p. 175–188. [10.1016/j.tecto.2006.01.021](https://doi.org/10.1016/j.tecto.2006.01.021)
- Casquet, C., Dahlquist, J.A., Verdecchia, S.O., Baldo, E.G., Galindo, C., Rapela, C.W., Pankhurst, R.J., Morales, M.M., Murra, J.A., and Fanning, C.M. 2018, Review of the Cambrian Pampean orogeny of Argentina; a displaced orogen formerly attached to the Saldania Belt of South Africa?. *Earth-Science Reviews*, v. 177, p. 209–225. [10.1016/j.earscirev.2017.11.013](https://doi.org/10.1016/j.earscirev.2017.11.013)
- Charrier, R., Pinto, L., and Rodríguez, M.P. 2007, Tectonostratigraphic evolution of the Andean Orogen in Chile. *The Geology of Chile*, p. 21–114. <https://pubs.geoscienceworld.org/gsl/books/book/1529/chapter-abstract/107218073/Tectonostratigraphic-evolution-of-the-Andean?redirectedFrom=fulltext>
- Clauoué-Long, J.C., Compston, W., Roberts, J., and Fanning, C.M. 1995, Two Carboniferous ages: A comparison of SHRIMP zircon dating with conventional zircon ages and 40Ar/39Ar analysis. in Berggren, W. A., Kent, D.V., Aubry, M.P., and Hardenbol, J. eds. *Geochronology, Time Scales and Global Stratigraphic Correlation*. <https://pubs.geoscienceworld.org/sepm/books/book/1041/chapter-standard/10528640/Two-Carboniferous-Ages-A-Comparison-of-Shrimp>
- Clift, P.D., and Hartley, A.J. 2007, Slow rates of subduction erosion and coastal underplating along the Andean margin of Chile and Peru. *Geology*, v. 35, no. 6, p. 503–506. [10.1130/G23584A.1](https://doi.org/10.1130/G23584A.1)
- Clift, P., and Vannucchi, P. 2004, Controls on tectonic accretion versus erosion in subduction zones: Implications for the origin and recycling of the continental crust. *Reviews of Geophysics*, v. 42, no. 2, [10.1029/2003RG000127](https://doi.org/10.1029/2003RG000127)
- Cloos, M. 1992, Thrust-type subduction-zone earthquakes and seamount asperities: A physical model for seismic rupture. *Geology*, v. 20, no. 7, p. 601–604. [10.1130/0091-7613\(1992\)020<0601:TTSZEA>2.3.CO;2](https://doi.org/10.1130/0091-7613(1992)020<0601:TTSZEA>2.3.CO;2)
- Cloos, M., and Shreve, R.L. 1988, Subduction-channel model of prism accretion, melange formation, sediment subduction, and subduction erosion at convergent plate margins: 1. Background and description. *Pure and Applied Geophysics*, v. 128, no. 3, p. 455–500. [10.1007/BF00874548](https://doi.org/10.1007/BF00874548)
- Cloos, M., and Shreve, R.L. 1996, Shear-zone thickness and the seismicity of Chilean and Marianas-type subduction zones. *Geology*, v. 24, no. 2, p. 107–110. [10.1130/0091-7613\(1996\)024<0107:SZTATS>2.3.CO;2](https://doi.org/10.1130/0091-7613(1996)024<0107:SZTATS>2.3.CO;2)
- Creixell, C. 2016, Geodynamics of late carboniferous–early permian forearc in north Chile (28° 30′–29° 30′ S). *Journal of the Geological Society*, v. 173, no. 5, p. 757–772. [10.1144/jgs2016-010](https://doi.org/10.1144/jgs2016-010)
- Creixell, C., Sepúlveda, F., Álvarez, J., Vásquez, P., and Velásquez, R. 2021, The Carboniferous onset of subduction at SW Gondwana revisited: Sedimentation and deformation processes along the late Paleozoic forearc of north Chile (21°–33° S). *Journal of South American Earth Sciences*, v. 107, p. 103149. [10.1016/j.jsames.2020.103149](https://doi.org/10.1016/j.jsames.2020.103149)
- Dahlquist, J.A., Cámara, M.M.M., Alasino, P.H., Pankhurst, R.J., Basei, M.A., Rapela, C.W., Moreno, J.A., Baldo, E.G., and Galindo, C. 2021, A review of Devonian–Carboniferous magmatism in the central region of Argentina, pre-Andean margin of SW Gondwana. *Earth-Science Reviews*, v. 221, p. 103781. [10.1016/j.earscirev.2021.103781](https://doi.org/10.1016/j.earscirev.2021.103781)
- Dalziel, I.W. 1991, Pacific margins of Laurentia and East Antarctica–Australia as a conjugate rift pair: Evidence and implications for an Eocambrian supercontinent. *Geology*, v. 19, no. 6, p. 598–601. [10.1130/0091-7613\(1991\)019<0598:PMOLAE>2.3.CO;2](https://doi.org/10.1130/0091-7613(1991)019<0598:PMOLAE>2.3.CO;2)
- Davidson, J., Mpodozis, C., Godoy, E., Herve, F., and Munoz, N. 1989, Jurassic accretion of a high buoyancy guyot in southernmost South America: The Diego Ramirez Islands.

- Andean Geology, v. 16, no. 2, p. 247–251. <http://www.andeangeology.cl/index.php/revista1/article/view/2366>
- Deckart, K., Hervé Allamand, F., Fanning, M., Ramírez, V., Calderón, M., and Godoy, E. 2014, U-Pb geochronology and Hf-O isotopes of zircons from the Pennsylvanian Coastal Batholith, south-central Chile. *Andean Geology*, v. 41, no. 1, p. 49–82. <http://andeangeology.cl/index.php/revista1/article/view/V41n1-a03>
- Delph, J.R., Thomas, A.M., and Levander, A. 2021, Subcretionary tectonics: Linking variability in the expression of subduction along the Cascadia forearc. *Earth and Planetary Science Letters*, v. 556, p. 116724. [10.1016/j.epsl.2020.116724](https://doi.org/10.1016/j.epsl.2020.116724)
- Dominguez, S., Malavieille, J., and Lallemand, S.E. 2000, Deformation of accretionary wedges in response to sea-mount subduction: Insights from sandbox experiments. *Tectonics*, v. 19, no. 1, p. 182–196. [10.1029/1999TC900055](https://doi.org/10.1029/1999TC900055)
- Ernst, W.G. 2011, Accretion of the Franciscan complex attending Jurassic–Cretaceous geotectonic development of northern and central California. *GSA Bulletin*, v. 123, no. 9–10, p. 1667–1678. [10.1130/B30398.1](https://doi.org/10.1130/B30398.1)
- Evans, B.W. 1990, Phase relations of epidote-blueschists. *Lithos*, v. 25, no. 1–3, p. 3–23. [10.1016/0024-4937\(90\)90003-J](https://doi.org/10.1016/0024-4937(90)90003-J)
- Fuenlabrada, J.M., Arenas, R., Martínez, S.S., García, F.D., and Castiñeiras, P. 2010, A peri-Gondwanan arc in NW Iberia: I: Isotopic and geochemical constraints on the origin of the arc—a sedimentary approach. *Gondwana Research*, v. 17, no. 2–3, p. 338–351. [10.1016/j.gr.2009.09.007](https://doi.org/10.1016/j.gr.2009.09.007)
- Geersen, J., Ranero, C.R., Barckhausen, U., and Reichert, C. 2015, Subducting seamounts control interplate coupling and seismic rupture in the 2014 Iquique earthquake area. *Nature Communications*, v. 6, no. 1, p. 1–6. [10.1038/ncomms9267](https://doi.org/10.1038/ncomms9267)
- Glodny, J., Echter, H., Collao, S., Ardiles, M., Burón, P., and Figueroa, O. 2008, Differential late paleozoic active margin evolution in South-Central Chile (37° S–40° S)—the Iñalhue fault zone. *Journal of South American Earth Sciences*, v. 26, no. 4, p. 397–411. [10.1016/j.jsames.2008.06.001](https://doi.org/10.1016/j.jsames.2008.06.001)
- Glodny, J., Lohrmann, J., Echter, H., Gräfe, K., Seifert, W., Collao, S., and Figueroa, O. 2005, Internal dynamics of a paleoaccretionary wedge: Insights from combined isotope tectonochronology and sandbox modelling of the South-Central Chilean forearc. *Earth and Planetary Science Letters*, v. 23, no. 1–2, p. 23–39. [10.1016/j.epsl.2004.12.014](https://doi.org/10.1016/j.epsl.2004.12.014)
- Grove, M., and Bebout, G.E. 1995, Cretaceous tectonic evolution of coastal southern California: Insights from the Catalina Schist. *Tectonics*, v. 14, no. 6, p. 1290–1308. [10.1029/95TC01931](https://doi.org/10.1029/95TC01931)
- Halama, R., and Konrad-Schmolke, M. 2015, Retrograde metasomatic effects on phase assemblages in an interlayered blueschist–greenschist sequence (Coastal Cordillera, Chile). *Lithos*, v. 216, p. 31–47. [10.1016/j.lithos.2014.12.004](https://doi.org/10.1016/j.lithos.2014.12.004)
- Heredia, N., García-Sansegundo, J., Gallastegui, G., Farias, P., Giacosa, R., Hongn, F., Tubía, J.M., Alonso, J.J., Busquets, P., Charrier, R., and Clariana, P. 2018, The pre-andean phases of construction of the southern andes basement in neoproterozoic–paleozoic times. The evolution of the Chilean–Argentinean Andes, p. 111–131. Springer:Cham. https://link.springer.com/chapter/10.1007/978-3-319-67774-3_5
- Hernández-Urbe, D., Palín, R.M., Cone, K.A., and Cao, W. 2020, Petrological implications of seafloor hydrothermal alteration of subducted mid-ocean ridge basalt. *Journal of Petrology*, v. 61, no. 9, p. ega086. [10.1093/petrology/egaa086](https://doi.org/10.1093/petrology/egaa086)
- Herron, M.M. 1988, Geochemical classification of terrigenous sands and shales from core or log data. *Journal of Sedimentary Research*, v. 58, no. 5, p. 820–829. [10.1306/212F8E77-2B24-11D7-8648000102C1865D](https://doi.org/10.1306/212F8E77-2B24-11D7-8648000102C1865D)
- Hervé, F. 1988, Late Paleozoic subduction and accretion in Southern Chile. *Episodes Journal of International Geoscience*, v. 11, no. 3, p. 183–188. [10.18814/epiiugs/1988/v11i3/005](https://doi.org/10.18814/epiiugs/1988/v11i3/005)
- Hervé, F., Calderón, M., Fanning, C.M., Pankhurst, R.J., and Godoy, E. 2013, Provenance variations in the Late Paleozoic accretionary complex of central Chile as indicated by detrital zircons. *Gondwana Research*, v. 23, no. 3, p. 1122–1135. [10.1016/j.gr.2012.06.016](https://doi.org/10.1016/j.gr.2012.06.016)
- Hervé, F., Calderón, M., Fanning, C.M., Pankhurst, R.J., and Navarro, J. 2020, U–pb SHRIMP detrital zircon dating of metamorphic rocks in north–central Chile (28°–33° S): Evidence for Carboniferous and Triassic metamorphism in a subduction setting. *Journal of South American Earth Sciences*, v. 103, p. 102767. [10.1016/j.jsames.2020.102767](https://doi.org/10.1016/j.jsames.2020.102767)
- Hervé, F., Greene, F., and Pankhurst, R.J. 1994, Metamorphosed fragments of oceanic crust in the upper Paleozoic Chonos accretionary complex, southern Chile. *Journal of South American Earth Sciences*, v. 7, no. 3–4, p. 263–270. [10.1016/0895-9811\(94\)90012-4](https://doi.org/10.1016/0895-9811(94)90012-4)
- Hervé, F., Kawashita, K., Munizaga, F., and Bassei, M. 1984, Rb–Sr isotopic ages from late Palaeozoic metamorphic rocks of central Chile. *Journal of the Geological Society*, v. 141, no. 5, p. 877–884. [10.1144/gsjgs.141.5.0877](https://doi.org/10.1144/gsjgs.141.5.0877)
- Heuret, A., Conrad, C.P., Funiello, F., Lallemand, S., and Sandri, L. 2012, Relation between subduction megathrust earthquakes, trench sediment thickness and upper plate strain. *Geophysical Research Letters*, v. 39, no. 5, [10.1029/2011GL050712](https://doi.org/10.1029/2011GL050712)
- Hicks, S.P., Rietbrock, A., Haberland, C.A., Ryder, I.M., Simons, M., and Tassara, A. 2012, The 2010 Mw 8.8 Maule, Chile earthquake: Nucleation and rupture propagation controlled by a subducted topographic high. *Geophysical Research Letters*, v. 39, no. 19, [10.1029/2012GL053184](https://doi.org/10.1029/2012GL053184)
- Hirano, N. 2006, Volcanism in response to plate flexure. *Science*, v. 313, no. 5792, p. 1426–1428. [10.1126/science.1128235](https://doi.org/10.1126/science.1128235)
- Hirano, N. 2011, Petit-spot volcanism: A new type of volcanic zone discovered near a trench. *Geochemical Journal*, v. 45, no. 2, p. 157–167. [10.2343/geochemj.1.0111](https://doi.org/10.2343/geochemj.1.0111)
- Hirano, N., Machida, S., Abe, N., Morishita, T., Tamura, A., and Arai, S. 2013, Petit-spot lava fields off the central Chile trench induced by plate flexure. *Geochemical Journal*, v. 47, no. 2, p. 249–257. [10.2343/geochemj.2.0227](https://doi.org/10.2343/geochemj.2.0227)
- Hu, J., Liu, L., and Gurnis, M. 2021, Southward expanding plate coupling due to variation in sediment subduction as a cause of Andean growth. *Nature Communications*, v. 12, no. 1, p. 1–9. [10.1038/s41467-021-27518-8](https://doi.org/10.1038/s41467-021-27518-8)
- Hyppolito, T. 2014, Metamorfismo y evolución tectónica del cinturón pareado permo-carbonífero en la región de Pichilemu, cordillera de la costa de Chile central, Doctoral dissertation, Universidad de Granada. <https://dialnet.unirioja.es/servlet/tesis?codigo=58080>
- Hyppolito, T., Angiboust, S., Juliani, C., Glodny, J., García-Casco, A., Calderón, M., and Chopin, C. 2016, Eclogite-, amphibolite- and blueschist-facies rocks from Diego de Almagro Island (Patagonia): Episodic accretion and thermal evolution of the

- Chilean subduction interface during the Cretaceous. *Lithos*, v. 264, p. 422–440. [10.1016/j.lithos.2016.09.001](https://doi.org/10.1016/j.lithos.2016.09.001)
- Hypolito, T., García-Casco, A., Juliani, C., Meira, V.T., and Hall, C. 2014, Late Paleozoic onset of subduction and exhumation at the western margin of Gondwana (Chilenia Terrane): Counterclockwise P–T paths and timing of metamorphism of deep-seated garnet–mica schist and amphibolite of Punta Sirena, coastal accretionary complex, central Chile (34 S). *Lithos*, v. 206, p. 409–434. <https://www.sciencedirect.com/science/article/pii/S0024493714002606>
- Hypolito, T., Juliani, C., García-Casco, A., Meira, V.T., Bustamante, A., and Hervé, F. 2014, The nature of the Palaeozoic oceanic basin at the southwestern margin of Gondwana and implications for the origin of the Chilenia terrane (Pichilemu region, central Chile). *International Geology Review*, v. 56, no. 9, p. 1097–1121. [10.1080/00206814.2014.919612](https://doi.org/10.1080/00206814.2014.919612)
- Jacques, G. 2013, Across-arc geochemical variations in the Southern Volcanic Zone, Chile (34.5–38.0 S): Constraints on mantle wedge and slab input compositions. *Geochimica et cosmochimica acta*, v. 123, p. 218–243. [10.1016/j.gca.2013.05.016](https://doi.org/10.1016/j.gca.2013.05.016)
- Jacques, G., Hauff, F., Hoernle, K., Jung, S., Kay, S.M., Garbe-Schönberg, D., and Bindeman, I. 2020, Sr–Nd–Pb–Hf–O isotopic constraints on the Neoproterozoic to Miocene upper and mid crust in central Chile and western Argentina and trench sediments (33°–35° S). *Journal of South American Earth Sciences*, v. 104, p. 102879. [10.1016/j.jsames.2020.102879](https://doi.org/10.1016/j.jsames.2020.102879)
- Ji, Y., Yoshioka, S., Manea, V.C., Manea, M., and Suenaga, N. 2019, Subduction thermal structure, metamorphism and seismicity beneath north-central Chile. *Journal of Geodynamics*, v. 129, p. 299–312. [10.1016/j.jog.2018.09.004](https://doi.org/10.1016/j.jog.2018.09.004)
- John, T., Scherer, E.E., Schenk, V., Herms, P., Halama, R., and Garbe-Schönberg, D. 2010, Subducted seamounts in an eclogite-facies ophiolite sequence: The Andean Raspas Complex, SW Ecuador, Contributions to Mineralogy and Petrology, v. 159, no. 2, p. 265–284. [10.1007/s00410-009-0427-0](https://doi.org/10.1007/s00410-009-0427-0)
- Kato, T.T., and Godoy, E. 2015, Middle to late Triassic mélangé exhumation along a pre-Andean transpressional fault system: Coastal Chile (26–42 S). *International Geology Review*, v. 57, no. 5–8, p. 606–628. [10.1080/00206814.2014.1002119](https://doi.org/10.1080/00206814.2014.1002119)
- Kato, T.T., Sharp, W.D., and Godoy, E. 2008, Inception of a Devonian subduction zone along the southwestern Gondwana margin: 40ar–39ar dating of eclogite–amphibolite assemblages in blueschist boulders from the Coastal Range of Chile (41° S). *Canadian Journal of Earth Sciences*, v. 45, no. 3, p. 337–351. [10.1139/E08-006](https://doi.org/10.1139/E08-006)
- Kay, S.M., Mpodozis, C., and Gardeweg, M. 2014, Magma sources and tectonic setting of Central Andean andesites (25.5–28 S) related to crustal thickening, forearc subduction erosion and delamination. *Geological Society Special Publications London*, v. 385, no. 1, p. 303–334. [10.1144/SP385.11](https://doi.org/10.1144/SP385.11)
- Kukowski, N., and Oncken, O. 2006, Subduction erosion—the “normal” mode of fore-arc material transfer along the Chilean margin?. in *The andes*, p. 217–236. Springer: Berlin, Heidelberg. https://link.springer.com/chapter/10.1007/978-3-540-48684-8_10
- Kukowski, N., Von Huene, R., Malavieille, J., and Lallemand, S.E. 1994, Sediment accretion against a buttress beneath the Peruvian continental margin at 12 S as simulated with sandbox modeling. *Geologische Rundschau*, v. 83, no. 4, p. 822–831. [10.1007/BF00251079](https://doi.org/10.1007/BF00251079)
- Lallemand, S.E., Malavieille, J., and Calassou, S. 1992, Effects of oceanic ridge subduction on accretionary wedges: Experimental modeling and marine observations. *Tectonics*, v. 11, no. 6, p. 1301–1313. [10.1029/92TC00637](https://doi.org/10.1029/92TC00637)
- Lallemand, S.E., Schnürle, P., and Malavieille, J. 1994, Coulomb theory applied to accretionary and nonaccretionary wedges: Possible causes for tectonic erosion and/or frontal accretion. *Journal of Geophysical Research: Solid Earth*, v. 99, no. B6, p. 12033–12055. [10.1029/94JB00124](https://doi.org/10.1029/94JB00124)
- Lamb, S., and Davis, P. 2003, Cenozoic climate change as a possible cause for the rise of the Andes. *Nature*, v. 425, no. 6960, p. 792–797. [10.1038/nature02049](https://doi.org/10.1038/nature02049)
- Li, J. 2018, Connections between subducted sediment, pore-fluid pressure, and earthquake behavior along the Alaska megathrust. *Geology*, v. 46, no. 4, p. 299–302. [10.1130/G39557.1](https://doi.org/10.1130/G39557.1)
- Lucassen, F., Trumbull, R., Franz, G., Creixell, C., Vázquez, P., Romer, R.L., and Figueroa, O. 2004, Distinguishing crustal recycling and juvenile additions at active continental margins: The Paleozoic to recent compositional evolution of the Chilean Pacific margin (36–41 S). *Journal of South American Earth Sciences*, v. 17, no. 2, p. 103–119. [10.1016/j.jsames.2004.04.002](https://doi.org/10.1016/j.jsames.2004.04.002)
- Lucassen, F., Wiedicke, M., and Franz, G. 2010, Complete recycling of a magmatic arc: Evidence from chemical and isotopic composition of quaternary trench sediments in Chile (36–40 S). *International Journal of Earth Sciences*, v. 99, no. 3, p. 687–701. [10.1007/s00531-008-0410-4](https://doi.org/10.1007/s00531-008-0410-4)
- Massonne, H.J., and Calderón, M. 2008, PT evolution of metapelites from the Guarguaraz complex, Argentina: Evidence for Devonian crustal thickening close to the western Gondwana margin. *Revista geológica de Chile*, v. 35. [10.4067/S0716-02082008000200002](https://doi.org/10.4067/S0716-02082008000200002)
- McDonough, W.F., and Sun, S.S. 1995, The composition of the Earth. *Chemical Geology*, v. 120, no. 3–4, p. 223–253. [10.1016/0009-2541\(94\)00140-4](https://doi.org/10.1016/0009-2541(94)00140-4)
- McLennan, S.M. 2001, Relationships between the trace element composition of sedimentary rocks and upper continental crust. *Geochemistry, Geophysics, Geosystems*, v. 2, no. 4, [10.1029/2000GC000109](https://doi.org/10.1029/2000GC000109)
- McLennan, S.M., and Taylor, S.R. 1991, Sedimentary rocks and crustal evolution: Tectonic setting and secular trends. *The Journal of Geology*, v. 99, no. 1, p. 1–21. [10.1086/629470](https://doi.org/10.1086/629470)
- Menant, A., Angiboust, S., and Gerya, T. 2019, Stress-driven fluid flow controls long-term megathrust strength and deep accretionary dynamics. *Scientific Reports*, v. 9, no. 1, p. 1–11. [10.1038/s41598-019-46191-y](https://doi.org/10.1038/s41598-019-46191-y)
- Menant, A., Angiboust, S., Gerya, T., Lacassin, R., Simoes, M., and Grandin, R. 2020, Transient stripping of subducting slabs controls periodic forearc uplift. *Nature Communications*, v. 11, no. 1, p. 1–10. [10.1038/s41467-020-15580-7](https://doi.org/10.1038/s41467-020-15580-7)
- Miura, R., Nakamura, Y., Koda, K., Tokuyama, H., and Coffin, M.F. 2004, “Rootless” serpentinite seamount on the southern Izu-Bonin forearc: Implications for basal erosion at convergent plate margins. *Geology*, v. 32, no. 6, p. 541–544. [10.1130/G20319.1](https://doi.org/10.1130/G20319.1)
- Moore, J.C., and Saffer, D. 2001, Updip limit of the seismogenic zone beneath the accretionary prism of southwest Japan: An effect of diagenetic to low-grade metamorphic processes

- and increasing effective stress. *Geology*, v. 29, no. 2, p. 183–186. [10.1130/0091-7613\(2001\)029<0183:ULOTSZ>2.0.CO;2](https://doi.org/10.1130/0091-7613(2001)029<0183:ULOTSZ>2.0.CO;2)
- Moreno, M. 2018, Chilean megathrust earthquake recurrence linked to frictional contrast at depth. *Nature Geoscience*, v. 11, no. 4, p. 285–290. [10.1038/s41561-018-0089-5](https://doi.org/10.1038/s41561-018-0089-5)
- Moreno, M., Haberland, C., Oncken, O., Rietbrock, A., Angiboust, S., and Heidbach, O. 2014, Locking of the Chile subduction zone controlled by fluid pressure before the 2010 earthquake. *Nature Geoscience*, v. 7, no. 4, p. 292–296. [10.1038/ngeo2102](https://doi.org/10.1038/ngeo2102)
- Muldashev, I.A., and Sobolev, S.V. 2020, What controls maximum magnitudes of giant subduction earthquakes? *Geochemistry, Geophysics, Geosystems*, v. 21, no. 9, p. e2020GC009145. [10.1029/2020GC009145](https://doi.org/10.1029/2020GC009145)
- Muñoz-Montecinos, J., Angiboust, S., Cambeses, A., and García-Casco, A. 2020, Multiple veining in a paleo-accretionary wedge: The metamorphic rock record of prograde dehydration and transient high pore-fluid pressures along the subduction interface (Western Series, central Chile). *Geosphere*, v. 16, no. 3, p. 765–786. [10.1130/GES02227.1](https://doi.org/10.1130/GES02227.1)
- Muñoz-Montecinos, J., Angiboust, S., and Garcia-Casco, A. 2021, Blueschist-facies paleo-earthquakes in a serpentinite channel (Zagros suture, Iran) enlighten seismogenesis in Mariana-type subduction margins. *Earth and Planetary Science Letters*, v. 573, p. 117135. [10.1016/j.epsl.2021.117135](https://doi.org/10.1016/j.epsl.2021.117135)
- Muñoz-Montecinos, J., Angiboust, S., Garcia-Casco, A., Glodny, J., and Bebout, G. 2021, Episodic hydrofracturing and large-scale flushing along deep subduction interfaces: Implications for fluid transfer and carbon recycling (Zagros Orogen, southeastern Iran). *Chemical Geology*, v. 571, p. 120173. [10.1016/j.chemgeo.2021.120173](https://doi.org/10.1016/j.chemgeo.2021.120173)
- Noda, A., Koge, H., Yamada, Y., Miyakawa, A., and Ashi, J. 2020, Subduction of trench-fill sediments beneath an accretionary wedge: Insights from sandbox analogue experiments. *Geosphere*, v. 16, no. 4, p. 953–968. [10.1130/GES02212.1](https://doi.org/10.1130/GES02212.1)
- Noda, A., and Sato, D. 2018, Submarine slope-fan sedimentation in an ancient forearc related to contemporaneous magmatism: The upper cretaceous izumi group, southwestern Japan. *Island Arc*, v. 27, no. 2, p. e12240. [10.1111/iar.12240](https://doi.org/10.1111/iar.12240)
- Obara, K., Hirose, H., Yamamizu, F., and Kasahara, K. 2004, Episodic slow slip events accompanied by non-volcanic tremors in southwest Japan subduction zone: Geophysical Research Letters, v. 31 23. [10.1029/2004GL020848](https://doi.org/10.1029/2004GL020848)
- Peacock, S.M., Wang, K., and McMahon, A.M. 2002, Thermal structure and metamorphism of subducting oceanic crust: Insight into Cascadia intraslab earthquakes. in Kirby, S., Wang, K., and Dunlop, S. eds. *The Cascadia subduction zone and related subduction systems: seismic structure, Intraslab Earthquakes and Processes, and Earthquake Hazards: Geological Survey of Canada Open File*, 4350.
- Pearce, J.A. 1996, A user's guide to basalt discrimination diagrams. Trace element geochemistry of volcanic rocks: Applications for massive sulphide exploration. Geological Association of Canada, Short Course Notes, v. 12, no. 79, p. 113. <https://cir.nii.ac.jp/crid/1573387451178072192>
- Pearce, J.A. 2008, Geochemical fingerprinting of oceanic basalts with applications to ophiolite classification and the search for Archean oceanic crust. *Lithos*, v. 100, no. 1–4, p. 14–48. [10.1016/j.lithos.2007.06.016](https://doi.org/10.1016/j.lithos.2007.06.016)
- Plank, T. 2014, April 17, The chemical composition of subducting sediments. in Rudnick, R.L., Holland, H.D., Turekian, K.K. eds. *The Crust, Treatise on Geochemistry*. 2nd ed., pp. p. 607–629. Elsevier-Pergamon: Oxford. <https://oceanrep.geomar.de/id/eprint/46757/>
- Platt, J.P. 1993, Exhumation of high-pressure rocks: A review of concepts and processes, *Terra Nova*. v. 5, no. 2, p. 119–133. [10.1111/j.1365-3121.1993.tb00237.x](https://doi.org/10.1111/j.1365-3121.1993.tb00237.x)
- Platt, J.P., Xia, H., and Schmidt, W.L. 2018, Rheology and stress in subduction zones around the aseismic/seismic transition. *Progress in Earth and Planetary Science*, v. 5, no. 1, p. 1–12. [10.1186/s40645-018-0183-8](https://doi.org/10.1186/s40645-018-0183-8)
- Plissart, G. 2019, Tectono-metamorphic evolution of subduction channel serpentinites from South-Central Chile. *Lithos*, v. 336, p. 221–241. [10.1016/j.lithos.2019.03.023](https://doi.org/10.1016/j.lithos.2019.03.023)
- Raimbourg, H., Augier, R., Famin, V., Gadenne, L., Palazzin, G., Yamaguchi, A., and Kimura, G. 2014, Long-term evolution of an accretionary prism: The case study of the Shimanto Belt, Kyushu, Japan. *Tectonics*, v. 33, no. 6, p. 936–959. [10.1002/2013TC003412](https://doi.org/10.1002/2013TC003412)
- Ramos, V.A. 2004, Cuyania, an exotic block to Gondwana: Review of a historical success and the present problems. *Gondwana Research*, v. 7, no. 4, p. 1009–1026. [10.1016/S1342-937X\(05\)71081-9](https://doi.org/10.1016/S1342-937X(05)71081-9)
- Ramos, V.A., Jordan, T.E., Allmendinger, R.W., Mpodozis, C., Kay, S.M., Cortés, J.M., and Palma, M. 1986, Paleozoic terranes of the central Argentine-Chilean Andes. *Tectonics*, v. 5, no. 6, p. 855–880. [10.1029/TC005i006p00855](https://doi.org/10.1029/TC005i006p00855)
- Ramos, C., Mechie, J., and Stiller, M. 2018, Reflection seismic images and amplitude ratio modelling of the Chilean subduction zone at 38.25 S. *Tectonophysics*, v. 747, p. 115–127. [10.1016/j.tecto.2018.10.007](https://doi.org/10.1016/j.tecto.2018.10.007)
- Rapalini, A.E., Geuna, S.E., Franceschinis, P.R., and Spagnuolo, C. M. 2018, Paleogeographic and kinematic constraints in the tectonic evolution of the Pre-Andean basement blocks. The evolution of the Chilean-Argentinean Andes, p. 83–109. *Springer Earth System Sciences: Springer, Cham*. [10.1007/978-3-319-67774-3_4](https://doi.org/10.1007/978-3-319-67774-3_4)
- Rapela, C.W. 2007, The Río de la Plata craton and the assembly of SW Gondwana. *Earth-Science Reviews*, v. 83, no. 1–2, p. 49–82. [10.1016/j.earscirev.2007.03.004](https://doi.org/10.1016/j.earscirev.2007.03.004)
- Rapela, C.W., Verdecchia, S.O., Casquet, C., Pankhurst, R.J., Baldo, E.G., Galindo, C., Murra, J.A., Dahlquist, J.A., and Fanning, C.M. 2016, Identifying Laurentian and SW Gondwana sources in the Neoproterozoic to early Paleozoic metasedimentary rocks of the Sierras Pampeanas: Paleogeographic and tectonic implications. *Gondwana Research*, v. 32, p. 193–212. [10.1016/j.gr.2015.02.010](https://doi.org/10.1016/j.gr.2015.02.010)
- Richter, P.P., Ring, U., Willner, A.P., and Leiss, B. 2007, Structural contacts in subduction complexes and their tectonic significance: The Late Palaeozoic coastal accretionary wedge of central Chile. *Journal of the Geological Society*, v. 164, no. 1, p. 203–214. [10.1144/0016-76492005-181](https://doi.org/10.1144/0016-76492005-181)
- Ring, U., and Layer, P.W. 2003, High-pressure metamorphism in the Aegean, eastern Mediterranean: Underplating and exhumation from the late cretaceous until the miocene to recent above the retreating hellenic subduction zone. *Tectonics*, v. 22, no. 3). [10.1029/2001TC001350](https://doi.org/10.1029/2001TC001350)
- Roser, B.P., and Korsch, R.J. 1988, Provenance signatures of sandstone-mudstone suites determined using discriminant function analysis of major-element data. *Chemical Geology*, v. 67, no. 1–2, p. 119–139. [10.1016/0009-2541\(88\)90010-1](https://doi.org/10.1016/0009-2541(88)90010-1)
- Rowe, C.D., Moore, J.C., Meneghini, F., and McKeirnan, A.W. 2005, Large-scale pseudotachylytes and fluidized

- cataclases from an ancient subduction thrust fault. *Geology*, v. 33, no. 12, p. 937–940. [10.1130/G21856.1](https://doi.org/10.1130/G21856.1)
- Ruff, L.J. 1989, Do trench sediments affect great earthquake occurrence in subduction zones?. *Pageoph*, v. 129, p. 263–282. [10.1007/BF00874629](https://doi.org/10.1007/BF00874629)
- Ruh, J.B., Kaus, B.J., and Burg, J.P. 2012, Numerical investigation of deformation mechanics in fold-and-thrust belts: Influence of rheology of single and multiple décollements. *Tectonics*, v. 31, no. 3). [10.1029/2011TC003047](https://doi.org/10.1029/2011TC003047)
- Ruh, J.B., Sallarès, V., Ranero, C.R., and Gerya, T. 2016, Crustal deformation dynamics and stress evolution during seamount subduction: High-resolution 3-D numerical modeling. *Journal of Geophysical Research: Solid Earth*, v. 121, no. 9, p. 6880–6902. [10.1002/2016JB013250](https://doi.org/10.1002/2016JB013250)
- Sanhueza, J., Yáñez, G., Barra, F., Maringue, J., Figueroa, R., and Sáez, E. 2021, Rheological, petrophysical and geometrical constraints of a subduction channel from a numerical model perspective: Insights from La Cabaña Paleozoic peridotites, Coastal Cordillera of south-central Chile. *Journal of South American Earth Sciences*, v. 103706, p. 103706. [10.1016/j.jsames.2021.103706](https://doi.org/10.1016/j.jsames.2021.103706)
- Scholl, D.W. 2019, Seismic imaging evidence that forearc underplating built the accretionary rock record of coastal North and South America. *Geological Magazine*, v. 158, no. 1, p. 104–117. [10.1017/S0016756819000955](https://doi.org/10.1017/S0016756819000955)
- Scholl, D.W., and von Huene, R. 2010, Subduction zone recycling processes and the rock record of crustal suture zones. *Canadian Journal of Earth Sciences*, v. 47, no. 5, p. 633–654. [10.1139/E09-061](https://doi.org/10.1139/E09-061)
- Scholz, C.H., and Small, C. 1997, The effect of seamount subduction on seismic coupling. *Geology*, v. 25, no. 6, p. 487–490. [10.1130/0091-7613\(1997\)025<0487:TEOSSO>2.3.CO;2](https://doi.org/10.1130/0091-7613(1997)025<0487:TEOSSO>2.3.CO;2)
- Spear, F.S., 1993, *Metamorphic Phase Equilibria and Pressure-Temperature-Time Paths*. Washington, D.C: Mineralogical Society of America. p. 799.
- Stern, R.J. 2002, Subduction zones. *Reviews of Geophysics*, v. 40, no. 4, p. 3–1. [10.1029/2001RG000108](https://doi.org/10.1029/2001RG000108)
- Sun, T., Saffer, D., and Ellis, S. 2020, Mechanical and hydrological effects of seamount subduction on megathrust stress and slip. *Nature Geoscience*, v. 13, no. 3, p. 249–255. [10.1038/s41561-020-0542-0](https://doi.org/10.1038/s41561-020-0542-0)
- Taylor, S. R., and McLennan, S. M. 1995, The geochemical evolution of the continental crust, *Reviews of geophysics*, v. 33, no. 2, p. 241–265. [10.1029/95RG00262](https://doi.org/10.1029/95RG00262)
- Tewksbury-Christle, C.M., and Behr, W.M. 2021, Constraints from exhumed rocks on the seismic signature of the deep subduction interface. *Geophysical Research Letters*, v. 48, no. 18). [10.1029/2021GL093831](https://doi.org/10.1029/2021GL093831)
- Thomas, W.A., and Astini, R.A. 2003, Ordovician accretion of the Argentine Precordillera terrane to Gondwana: A review. *Journal of South American Earth Sciences*, v. 16, no. 1, p. 67–79. [10.1016/S0895-9811\(03\)00019-1](https://doi.org/10.1016/S0895-9811(03)00019-1)
- Tobin, H.J., and Saffer, D.M. 2009, Elevated fluid pressure and extreme mechanical weakness of a plate boundary thrust. Nankai Trough Subduction Zone, *Geology*, v. 37, no. 8, p. 679–682. [10.1130/G25752A.1](https://doi.org/10.1130/G25752A.1)
- Torres-Roldan, R.L., Garcia-Casco, A., and Garcia-Sanchez, P.A. 2000, Cspace: An integrated workplace for the graphical and algebraic analysis of phase assemblages on 32-bit Wintel platforms. *Computers & Geosciences*, v. 26, no. 7, p. 779–793. [10.1016/S0098-3004\(00\)00006-6](https://doi.org/10.1016/S0098-3004(00)00006-6)
- Trouw, R.A.J., Simoes, L.S.A., and Valladares, C.S. 1998, Metamorphic evolution of a subduction complex, South Shetland Islands, Antarctica. *Journal of Metamorphic Geology*, v. 16, no. 4, p. 475–490. [10.1111/j.1525-1314.1998.00151.x](https://doi.org/10.1111/j.1525-1314.1998.00151.x)
- Uchida, N., Kirby, S.H., Okada, T., Hino, R., and Hasegawa, A. 2010, Supraslab earthquake clusters above the subduction plate boundary offshore Sanriku, northeastern Japan: Seismogenesis in a graveyard of detached seamounts?: *Journal of Geophysical Research: Solid Earth*, v. 115, B9. [10.1029/2009JB006797](https://doi.org/10.1029/2009JB006797)
- Verdecchia, S.O., Casquet, C., Baldo, E.G., Pankhurst, R.J., Rapela, C.W., Fanning, M., and Galindo, C. 2011, Mid-to late Cambrian docking of the Río de la Plata craton to southwestern Gondwana: Age constraints from U–Pb SHRIMP detrital zircon ages from Sierras de Ambato and Velasco (Sierras Pampeanas, Argentina). *Journal of the Geological Society*, v. 168, no. 4, p. 1061–1071. [10.1144/0016-76492010-143](https://doi.org/10.1144/0016-76492010-143)
- Vervoort, J.D., Plank, T., and Prytulak, J. 2011, The Hf–Nd isotopic composition of marine sediments. *Geochimica et cosmochimica acta*, v. 75, no. 20, p. 5903–5926. [10.1016/j.gca.2011.07.046](https://doi.org/10.1016/j.gca.2011.07.046)
- Völker, D., Reichel, T., Wiedicke, M., and Heubeck, C. 2008, Turbidites deposited on Southern Central Chilean seamounts: Evidence for energetic turbidity currents. *Marine Geology*, v. 251, no. 1–2, p. 15–31. [10.1016/j.margeo.2008.01.008](https://doi.org/10.1016/j.margeo.2008.01.008)
- von Huene, R., Miller, J.J., and Krabbenhoef, A. 2021, The Alaska convergent margin backstop splay fault zone, a potential large tsunami generator between the frontal prism and continental framework. *Geochemistry, Geophysics, Geosystems*, v. 22, no. 1, p. e2019GC008901. [10.1029/2019GC008901](https://doi.org/10.1029/2019GC008901)
- Wakabayashi, J. 2017, Structural context and variation of ocean plate stratigraphy, Franciscan Complex, California: Insight into mélange origins and subduction-accretion processes. *Progress in Earth and Planetary Science*, v. 4, no. 1, p. 1–23. [10.1186/s40645-017-0132-y](https://doi.org/10.1186/s40645-017-0132-y)
- Wakita, K. 2019, Tectonic setting required for the preservation of sedimentary mélanges in Palaeozoic and Mesozoic accretionary complexes of southwest Japan. *Gondwana Research*, v. 74, p. 90–100. [10.1016/j.gr.2019.03.006](https://doi.org/10.1016/j.gr.2019.03.006)
- Wang, K., and Bilek, S.L. 2011, Do subducting seamounts generate or stop large earthquakes?. *Geology*, v. 39, no. 9, p. 819–822. [10.1130/G31856.1](https://doi.org/10.1130/G31856.1)
- Whitney, D.L., and Evans, B.W. 2010, Abbreviations for names of rock-forming minerals. *American Mineralogist*, v. 95, no. 1, p. 185–187. [10.2138/am.2010.3371](https://doi.org/10.2138/am.2010.3371)
- Williams, I. S., and Claesson, S. 1987, Isotopic evidence for the Precambrian provenance and Caledonian metamorphism of high grade paragneisses from the Seve Nappes, Scandinavian Caledonides: II. Ion microprobe zircon U–Th–Pb. *Contributions to mineralogy and petrology*, v. 97, no. 2, p. 205–217.
- Willner, A.P. 2005, Pressure–temperature evolution of a Late Palaeozoic paired metamorphic belt in North–Central Chile (34°–35° 30' S). *Journal of Petrology*, v. 46, no. 9, p. 1805–1833. [10.1093/petrology/egi035](https://doi.org/10.1093/petrology/egi035)
- Willner, A. P., Gerdas, A., and Massonne, H. J. (2008). History of crustal growth and recycling at the Pacific convergent margin of South America at latitudes 29–36 S revealed by a U–Pb and Lu–Hf isotope study of detrital zircon from late

- Paleozoic accretionary systems. *Chemical geology*, v. 253, no. 3–4, p. 114–129.
- Willner, A.P., Gerdes, A., Massonne, H.J., Schmidt, A., Sudo, M., Thomson, S.N., and Vujovich, G. 2011, The geodynamics of collision of a microplate (Chilenia) in Devonian times deduced by the pressure–temperature–time evolution within part of a collisional belt (Guarguaraz Complex, W-Argentina). *Contributions to Mineralogy and Petrology*, v. 162, no. 2, p. 303–327. [10.1007/s00410-010-0598-8](https://doi.org/10.1007/s00410-010-0598-8)
- Willner, A.P., Glodny, J., Gerya, T.V., Godoy, E., and Massonne, H.J. 2004, A counterclockwise PTt path of high-pressure/low-temperature rocks from the Coastal Cordillera accretionary complex of south-central Chile: Constraints for the earliest stage of subduction mass flow. *Lithos*, v. 75, no. 3–4, p. 283–310. [10.1016/j.lithos.2004.03.002](https://doi.org/10.1016/j.lithos.2004.03.002)
- Willner, A.P., Thomson, S.N., Kröner, A., Wartho, J.A., Wijbrans, J.R., and Hervé, F. 2005, Time markers for the evolution and exhumation history of a Late Palaeozoic paired metamorphic belt in North–Central Chile (34°–35° 30' S). *Journal of Petrology*, v. 46, no. 9, p. 1835–1858. [10.1093/petrology/egi036](https://doi.org/10.1093/petrology/egi036)
- Wilson, T.J., Hanson, R.E., and Grunow, A.M. 1989, Multistage melange formation within an accretionary complex, Diego Ramirez Islands, southern Chile. *Geology*, v. 17, no. 1, p. 11–14. [10.1130/0091-7613\(1989\)017<0011:MMFWAA>2.3.CO;2](https://doi.org/10.1130/0091-7613(1989)017<0011:MMFWAA>2.3.CO;2)
- Winchester, J.A., and Floyd, P.A. 1977, Geochemical discrimination of different magma series and their differentiation products using immobile elements. *Chemical Geology*, v. 20, p. 325–343. [10.1016/0009-2541\(77\)90057-2](https://doi.org/10.1016/0009-2541(77)90057-2)
- Xia, H., and Platt, J.P. 2017, Structural and rheological evolution of the Laramide subduction channel in southern California. *Solid Earth*, v. 8, no. 2, p. 379–403. [10.5194/se-8-379-2017](https://doi.org/10.5194/se-8-379-2017)
- Yamamoto, J., Hirano, N., and Kurz, M.D. 2020, Noble gas isotopic compositions of seamount lavas from the central Chile trench: Implications for petit-spot volcanism and the lithosphere asthenosphere boundary. *Earth and Planetary Science Letters*, v. 552, p. 116611. [10.1016/j.epsl.2020.116611](https://doi.org/10.1016/j.epsl.2020.116611)
- Yang, H., Liu, Y., and Lin, J. 2013, Geometrical effects of a subducted seamount on stopping megathrust ruptures. *Geophysical Research Letters*, v. 40, no. 10, p. 2011–2016. [10.1002/grl.50509](https://doi.org/10.1002/grl.50509)
- Yang, G., Li, Y., Xiao, W., and Tong, L. 2015, OIB-type rocks within West Junggar ophiolitic mélanges: Evidence for the accretion of seamounts. *Earth-Science Reviews*, v. 150, p. 477–496. [10.1016/j.earscirev.2015.09.002](https://doi.org/10.1016/j.earscirev.2015.09.002)
- Ye, S., Flueh, E.R., Klaeschen, D., and Von Huene, R. 1997, Crustal structure along the EDGE transect beneath the Kodiak shelf off Alaska derived from OBH seismic refraction data. *Geophysical Journal International*, v. 130, no. 2, p. 283–302. [10.1111/j.1365-246X.1997.tb05648.x](https://doi.org/10.1111/j.1365-246X.1997.tb05648.x)
- Žák, J., Svojtka, M., Hajná, J., and Ackerman, L. 2020, Detrital zircon geochronology and processes in accretionary wedges. *Earth-Science Reviews*, v. 103214, p. 103214. [10.1016/j.earscirev.2020.103214](https://doi.org/10.1016/j.earscirev.2020.103214)